

**CHARACTERIZATION OF LYSOZYME ADSORPTION  
IN CELLULOSIC CHROMATOGRAPHIC PARTICLES  
USING SMALL-ANGLE NEUTRON SCATTERING**

by

Stijn Koshari

A thesis submitted to the Faculty of the University of Delaware in partial  
fulfillment of the requirements for the degree of Master of Chemical Engineering

Spring 2014

© 2014 Stijn Koshari  
All Rights Reserved

UMI Number: 1562392

All rights reserved

INFORMATION TO ALL USERS

The quality of this reproduction is dependent upon the quality of the copy submitted.

In the unlikely event that the author did not send a complete manuscript and there are missing pages, these will be noted. Also, if material had to be removed, a note will indicate the deletion.



UMI 1562392

Published by ProQuest LLC (2014). Copyright in the Dissertation held by the Author.

Microform Edition © ProQuest LLC.

All rights reserved. This work is protected against unauthorized copying under Title 17, United States Code



ProQuest LLC.  
789 East Eisenhower Parkway  
P.O. Box 1346  
Ann Arbor, MI 48106 - 1346

**CHARACTERIZATION OF LYSOZYME ADSORPTION  
IN CELLULOSIC CHROMATOGRAPHIC PARTICLES  
USING SMALL-ANGLE NEUTRON SCATTERING**

by

Stijn Koshari

Approved:

---

Abraham M. Lenhoff, Ph.D.  
Professor in charge of thesis on behalf of the Advisory Committee

Approved:

---

Norman J. Wagner, Ph.D.  
Professor in charge of thesis on behalf of the Advisory Committee

Approved:

---

Abraham M. Lenhoff, Ph.D.  
Chair of the Department of Chemical and Biomolecular Engineering

Approved:

---

Babatunde A. Ogunnaike, Ph.D.  
Dean of the College of Engineering

Approved:

---

James G. Richards, Ph.D.  
Vice Provost for Graduate and Professional Education

## ACKNOWLEDGMENTS

‘Dare to be first.’ is what the university keeps telling me, and from the first time I heard it, at the international student orientation during one of my first days in the USA, it felt very appropriate. It is difficult to express how great of an experience it has been, to be the first student to participate in the new Chemical Engineering dual degree program between the KU Leuven and the University of Delaware. It has truly changed my life quite a bit. It has opened a future for me which I could not anticipate when I first started my Chemical Engineering studies. To be first might sometimes be a challenge, but it is certainly a huge privilege and a thrilling experience. With a simple smile and severe satisfaction I can promote this program to all the students who glance across the sea and wonder if they dare...

There have many great people who have helped me to get here and laid out the path for me, and to be honest, without much effort from myself. So, firstly, I want to thank all those people who have contributed to get this program running and who have guided me along the way: Professor Paula Moldenaers, Professor Peter Van Puyvelde, Anouck Brouwers, Kathie Young, and appropriately, Professor Eric Furst. I especially want to thank Professor Bramie Lenhoff and Professor Norm Wagner for not only contributing to the program, but also for being my advisors. They didn’t just mentor me with my studies and research, but offered help and support for someone far from home. In addition, the Lenhoff and Wagner research groups have been a fantastic bunch of people to work with. Specifically, I’d like to extend my thanks to Dan Greene, Jim Angelo, Doug Godfrin, and Simon Rogers for their help with my thesis

work, and the execution of the contrast match experiment that initiated this work. Furthermore, the NIST Center for Neutron Research in general has been invaluable by providing me the time required to perform my experiment. Matt Wasbrough, Paul Butler, and Yun Liu, in particular, have been kind to lend me their time and expertise.

I cannot express enough my deep gratitude to my parents and the rest of my family and friends who have supported my stay in the USA. They have always been there for me, they have always paved the paths towards my dreams, they have always dared me to be first. I would like to acknowledge my friends in the USA, and the whole UD Ballroom Dance Team, for providing me a home when I was far away from my own.

May this thesis be a worthy first, and if not a pleasure, at least not too much of a burden to read either.

But first, a kiss to the one who'll always come first.

## TABLE OF CONTENTS

LIST OF TABLES .....	vii
LIST OF FIGURES .....	viii
NOMENCLATURE .....	xi
ABSTRACT .....	xiv

### Chapter

1	INTRODUCTION AND BACKGROUND .....	1
1.1	Protein Chromatography .....	1
1.2	Polymer-Derivatized Stationary Phases .....	3
1.3	Small-Angle Neutron Scattering .....	4
1.4	Thesis Objectives and Outline .....	7
2	EXPERIMENTAL METHODS .....	10
2.1	Materials .....	10
2.1.1	Buffers .....	10
2.1.2	Protein solutions .....	11
2.1.3	Stationary phase .....	11
2.2	Sample Preparation .....	11
2.2.1	Contrast matching experiment .....	11
2.2.2	Protein adsorption experiment .....	12
2.3	Small-Angle Neutron Scattering .....	13
2.3.1	Contrast matching experiment .....	13
2.3.2	Protein adsorption experiment .....	13
3	DATA ACQUISITION AND REDUCTION .....	15
3.1	Sample Compositions .....	15
3.2	Small-Angle Neutron Scattering Spectra .....	19
3.3	Removal of the Incoherent Background .....	20
3.4	Scaling of the Spectra .....	23

3.4.1	Contrast matching experiment.....	23
3.4.2	Protein adsorption experiment.....	27
4	PARTICLE MODELING.....	30
4.1	Introduction .....	30
4.2	Model Construction .....	33
4.3	The Generalized Guinier-Porod Model .....	36
5	PROTEIN ADSORPTION DATA ANALYSIS .....	38
5.1	Comparison of Spectra .....	38
5.2	Background.....	42
5.3	Scaling .....	46
5.4	Protein Monomers .....	47
5.5	Protein Adsorption.....	53
6	CONCLUSIONS AND FUTURE WORK.....	58
	REFERENCES .....	61
	Appendix	
	REPRINT PERMISSION LETTERS.....	66

## LIST OF TABLES

Table 1:	Overview of the contrast match samples.....	15
Table 2:	Overview of adsorption values in the protein adsorption experiments. ..	16
Table 3:	Detailed protein adsorption sample compositions.....	18
Table 4:	Experimentally determined, incoherent background values from the Porod plot. ....	24
Table 5:	Experimentally obtained scaling factors for the contrast matching samples, relative to sample E. ....	26
Table 6:	Experimentally obtained scaling factors for the protein adsorption samples, relative to sample E. ....	29
Table 7:	Chemical formula and incoherent scattering cross-sections for the different compounds as obtained from the NIST neutron activation and scattering calculator [18]. ....	43
Table 8:	Measured values for the incoherent background $d\Sigma d\Omega_{inc}$ for the protein adsorption experiment, along with calculated values in the cases of single and dominant multiple scattering. The ratios between the values are included. In addition, the transmission is given. ....	45
Table 9:	Values of the experimental scaling factors $S$ , along with the calculated values of the contrast factor $\Delta\beta^2$ . In addition, the D2O: H2O fractions, necessary for the calculation, are included.....	48
Table 10:	Predicted and actual protein concentrations in the samples. The ratio is also included.....	52
Table 11:	Experimentally obtained values for the fractal dimension of the protein adsorption contribution, along with the adsorption $q$ and the TIS. ....	55



## LIST OF FIGURES

Figure 1:	Adsorbed amounts in the protein adsorption samples as a function of supernatant concentration. The TIS values shown are approximate. Sample numbers are indicated.....	18
Figure 2:	Scattering spectra after basic reduction for the contrast matching samples. ....	20
Figure 3:	Scattering spectra after basic reduction for the protein adsorption samples. ....	21
Figure 4:	Porod plots for the contrast matching samples (left) and protein adsorption samples (right). The incoherent background $B$ can be determined from the slope of the linear fit (red). ....	22
Figure 5:	Illustration of the experimentally determined background values of the scattering spectra for the contrast matching samples (left) and protein adsorption samples (right). ....	22
Figure 6:	Scattering spectra after subtraction of the incoherent background. For display clarity, all spectra have been given the same background value. ....	24
Figure 7:	Scaled scattering spectra for the contrast matching experiment. ....	26
Figure 8:	Square root of the scaling factors as a function of the D2O: H2O fraction in the sample solution (blue). To get a linear fit (red), some points have to be inverted to take the sign into account. The contrast match point (CMP) is found where the scaling factor is zero. ....	27
Figure 9:	Illustration of how the scattering spectra are parallel and linear in the intermediate- $Q$ region ( $0.02 \leq Q \leq 0.03$ ). ....	28
Figure 10:	Scaled scattering spectra for the protein adsorption experiment. ....	29

Figure 11:	Illustration of how different models fit the SANS experimental data of cellulosic resin particles in deuterated water (sample E). The models are described in the text. Note that the Ornstein-Zernike and generalized Ornstein-Zernike models are fit only to the intermediate- and high- $Q$ regions ( $Q > 0.017 \text{ \AA}^{-1}$ ). All model parameters are kept adjustable for these fits.....	32
Figure 12:	Schematic diagram of the spectrum for normal polymer gels [16]. .....	33
Figure 13:	Comparison of the reduced spectra (with background correction and scaling) for the protein adsorption samples and the scattering from pure resin particles (sample E). .....	40
Figure 14:	Scattering spectra after subtraction of the pure resin particle scattering spectrum (blue) from the total coherent scattering spectra. The result represents the change in scattering caused by the addition of protein to the system. Two contributions are identified: scattering from the protein monomers in the high- $Q$ region and a change in structure in the low- $Q$ region.....	41
Figure 15:	Comparison of the experimentally measured incoherent background values with the calculated ones for the protein adsorption experiment, assuming single scattering. The red symbols represent outlier samples (sample 7 and sample 10). The blue line is a linear least-squares fit through the origin (excluding the outliers).....	45
Figure 16:	Comparison of the experimentally measured incoherent background values with the calculated ones for the protein adsorption experiment, assuming dominant multiple scattering. The red symbols represent outlier samples (sample 7 and sample 10). The blue line is a linear least-squares fit through the origin (excluding the outliers).....	46
Figure 17:	Comparison of the experimentally measured scaling factor $S$ values with the calculated contrast factors $\Delta\beta^2$ for the protein adsorption experiment. The red symbols represent outlier samples (sample 7 and sample 10). The blue line is a linear least squares fit (excluding the outliers).....	48
Figure 18:	Scattering spectra after subtraction of the pure resin particle scattering spectrum from the total coherent scattering spectra. The pure resin particle spectrum is first reduced by a factor 0.9 to negate the artifact due to the subtraction and scaling assumptions. The protein form factor as calculated by CRYSON for a $4.5 \times 10^{-6}$ mole/mL solution is shown in magenta. ....	50

Figure 19:	Fitting of the protein form factor spectra as calculated by CRYSON (red) to the experimentally obtained protein monomer contributions for the protein adsorption experiment. ....	52
Figure 20:	Comparison of the predicted protein concentrations (via CRYSON and least-squares fitting) with the actual sample concentrations for the protein adsorption experiment. The red symbols represent outlier samples (sample 7 and sample 10). The blue line is a linear least-squares fit through the origin (excluding the outliers). ....	53
Figure 21:	Linear fitting (red) of the fractal dimension of the protein adsorption contribution to the total coherent scattering in the protein adsorption experiment. ....	55
Figure 22:	Comparison of the experimentally measured fractal dimension of the protein adsorption contribution with the protein adsorption $q$ . The red symbols represent outlier samples (sample 7 and sample 10). ....	56
Figure 23:	Comparison of the experimentally measured fractal dimension of the protein adsorption contribution with the TIS. The red symbols represent outlier samples (sample 7 and sample 10). ....	56
Figure 24:	SEM images of Q HyperCel chemically fixed with OsO <sub>4</sub> , without (left) and with (right) adsorption of approximately 50% of the maximum capacity of $\beta$ -lactoglobulin [19], [20]. ....	57

## NOMENCLATURE

$A$	exposed sample area [ $\text{cm}^2$ ]
$B$	incoherent background scattering [ $\text{cm}^{-1}$ ]
$c$	compound concentration in the sample [ $\text{g/mL}$ ]
$C$	final protein concentration in the sample supernatant [ $\text{mg/mL}$ ]
$C_0$	initial protein concentration in the sample solution [ $\text{mg/mL}$ ]
CM	contrast matching
CMP	contrast match point
$d$	sample thickness [ $\text{cm}$ or $\text{mm}$ ]
$D$	fractal dimension $[-]$
$f_{\text{D}_2\text{O}}$	mole fraction $\text{D}_2\text{O}$ [mole %]
hpv	hydrated particle volume
$I$	scattering intensity [ $\text{counts s}^{-1}$ or $\text{cm}^{-1}$ ]
$I_0$	neutron flux [ $\text{counts s}^{-1}\text{cm}^{-2}$ ]
IEC	ion exchange chromatography
ISEC	inverse size-exclusion chromatography
$k$	Boltzmann constant [ $\text{J/K}$ ]
$K_N$	neutron calibration constant [ $\text{counts s}^{-1}$ ]
$K_{os}$	osmotic compressional modulus [ $\text{Pa}$ ]
$L$	real-space length [ $\text{\AA}$ ]
$m$	Porod exponent $[-]$
MW	molecular weight [ $\text{kD}$ ]

NSE	neutron spin echo
PA	protein adsorption
PDB	Protein Data Bank
PDM	polymer-derivatized material
$q$	adsorbed protein concentration [mg/mL hpv]
$Q$	momentum transfer vector (inverse-space) [ $\text{\AA}^{-1}$ ]
$r$	distance between sample and detector element [cm]
$R_g$	radius of gyration [ $\text{\AA}$ ]
$S$	contrast scaling factor [–]
SANS	small-angle neutron scattering
SDD	sample-to-detector distance [m]
SEM	scanning electron microscopy
SLS	scattering length density
$T$	transmission [–], or temperature [K]
TIS	total ionic strength [mM]
$V$	exposed sample volume [ $\text{cm}^3$ ], or total sample solution volume [mL]
$V_m$	hydrated particle volume (hpv) [mL hpv]
$\beta$	scattering length density [ $\text{\AA}^{-2}$ ]
$\Delta a$	area of a detector element [ $\text{cm}^2$ ]
$\Delta\beta^2$	contrast factor [ $\text{\AA}^{-4}$ ]
$\varepsilon$	detector counting efficiency [–]

$2\theta$	deflection angle between scattered neutrons and incident beam [—]
$\lambda$	neutron wavelength [Å]
$\mu$	linear attenuation coefficient of the neutron beam on passing through the sample [ $\text{cm}^{-1}$ ]
$\xi$	correlation length of polymer density fluctuations in a solution [Å]
$\Xi$	mean size of the static nonuniformities in a polymer gel [Å]
$\sigma_{\text{inc}}$	incoherent scattering cross-section [b]
$\Sigma_{\text{inc}}$	incoherent cross-section of a compound [ $\text{cm}^{-1}/(\text{g/mL})$ ]
$\left(\frac{d\Sigma}{d\Omega}\right)$	scattering cross-section normalized to unit sample volume [ $\text{cm}^{-1}$ ]
$\varphi$	polymer volume fraction [—]

## ABSTRACT

Polymer-derivatized chromatographic media (PDM) for protein separation have been shown to display clear benefits in key measures of performance compared to conventional media. However, mechanistic understanding of protein mobility in these media is limited, and more experimental research is necessary to provide the insight necessary to develop and validate models to design these media and the processes in which they are used.

Small-angle neutron scattering (SANS) is an entirely novel way to study and characterize these systems. As a first, preliminary feasibility study, the thesis discusses the difference between the SANS spectra from chromatographic media with and without adsorbed protein. In particular, we look at the adsorption of lysozyme on cellulosic S HyperCel (Pall Corporation) particles.

Contrast matching techniques are not viable for studying these systems, as the scattering length densities of the materials are too similar. Instead, we offer a framework that allows quantitative analysis of the protein adsorption by direct comparison of the scattering spectra before and after adsorption. To support this framework, reduction techniques like background removal and scaling are provided to allow quantitative comparison of the data, in addition to a theoretically derived model for the scattering from cellulosic gel-like particles.

The scattering spectrum from the particles with adsorbed protein has three contributions: (1) the pure particle without adsorbed protein, as captured by the

theoretically derived model; (2) the form factor of protein monomers, which can be seen at high values of the momentum transfer vector  $Q$ ; and (3) the change in the fractal-like structure of the media evident at low  $Q$  upon protein adsorption. The intermediate- $Q$  region of the scattering spectrum is not influenced by the adsorption of protein. These contributions are investigated for different protein loadings of the resin particles and successfully linked to the sample composition. The sample incoherent background can be predicted from the sample composition, and the total concentration of protein in the sample can be accurately acquired from the SANS spectrum. The findings support the idea that protein adsorption is uniform and leads to a virtual densification of the cellulosic gel-like particle structure.

To conclude, it is clear that SANS is capable of probing these structures, and that it can provide additional information on protein adsorption when analyzed within the context of the model framework developed in the thesis.



## **Chapter 1**

### **INTRODUCTION AND BACKGROUND**

#### **1.1 Protein Chromatography**

Protein purification requires obtaining a pure product from a complex and dilute mixture, usually requiring an elaborate process. Separation of a protein from a mixture is highly dependent on the physical and chemical properties of the individual protein. Consequently, the different varieties of proteins cannot be purified by the same single, simple procedure [1], and the ideal separation method for one protein may fail to purify another protein, especially if the starting mixtures are very different. The purification method also depends on the required final state of the separated protein. Depending on the application, the final product might be dilute and relatively impure, or highly concentrated and extremely pure, as is often required in the pharmaceutical industry. Indeed, protein purification does not only involve the removal of contaminants, but also the concentration, stabilization, and preparation for the intended application.

A variety of operations have been used to separate protein mixtures. One way to purify proteins is to rely on their relative solubility. Methods such as protein crystallization or fractional precipitation are still regularly used for separation of gross impurities, membrane proteins and nucleic acids [1]. Another way is taking advantage of the selective adsorption of proteins to a range of solid materials. Protein chromatography relies on this second separation mechanism.

Chromatography is a widely applied separation technique in which the mobile phase that has to be purified is carried through a column containing a stationary phase. The various constituents of the mobile phase differ in affinity for the stationary phase. Consequently, the constituents are retained by the stationary phase to varying degrees, leading to separation due to differences in the time taken to traverse the column length. Chromatographic separation of protein mixtures has become a widespread method for the recovery and purification of proteins in downstream biotechnological processes [2]. Liquid chromatography offers mild separation conditions, a high degree of resolution, and diverse adsorption mechanisms [3]. However, the resolution offered by this technique comes at a significant cost both in development and operation, as acquisition and operation of the materials and methods is expensive [4]. Depending on the process, the acquisition of materials can contribute up to 10% of the total downstream processing costs [5]. The total purification process – including steps like chromatography, centrifugation, filtration, buffer exchange, and freeze drying – may represent as much as 80% of the production cost of biotherapeutics [6], [7].

Chromatography remains the main separation technique in downstream processing in the biotechnological industry, although its limited efficiency and the consequent development of non-chromatographic alternatives has been the subject of recent research [8]–[10]. Virtually all protein purification processes are developed around at least one chromatographic step [11]. Karlsson *et al.* [12] report an average of about three chromatographic steps in each protein production process, and about 40% of these steps are ion exchange chromatography (IEC) [8].

Consequently, there is a large driving force to increase the efficiency of protein chromatography and find new methods to reduce costs. A major component of this

continuous innovation is the development and characterization of novel chromatographic materials and ligands.

## **1.2 Polymer-Derivatized Stationary Phases**

A wide range of chromatographic techniques has been developed, employing varying stationary phases to exploit different protein properties such as size, charge, hydrophobicity, and biospecific interaction [1]. These chromatographic techniques include size exclusion chromatography (which does not rely on adsorption), affinity chromatography, ion exchange chromatography, and hydrophobicity based chromatography. The stationary phases available for use in preparative chromatography of proteins cover different base matrices, pore structures, and functional ligands or elements. As such, the constitution of the stationary phase strongly determines the particular performance of liquid chromatography [3]. Oliveira *et al.* [6] list the general requirements for an ideal stationary phase as follows: high specificity, absence of hydrophobic binding sites, good chemical stability, good mechanical rigidity, high binding capacity, good recoverability, high reproducibility, and low cost. Typically, chromatography is performed in packed beds filled with the stationary phase in the form of spherical porous particles in which the adsorption process occurs mainly in the interior [11]. The chromatographic resin particles are porous, rigid, or semi-rigid with a size range of about 20 – 120  $\mu\text{m}$  [4].

Recently, there has been significant growth in stationary phases that are polymer-derivatized or -functionalized [5], [8]. The largest class of these materials are used in ion exchange chromatography. In contrast to traditional stationary phases – which have wide, easily-accessible pores – the base matrix of these polymer-derivatized materials (PDMs) is derivatized to add a covalently attached or grafted

polymer layer or, sometimes, a hydrogel that fills the pore space [8]. Since conventional and polymer-derivatized media are operated in the same way, they are generally analyzed within the same phenomenological framework, without clear distinction [8]. However, PDMs have been shown to display clear benefits in key measures of performance compared to conventional media, comprising much higher capacities and faster mass transport rates [11]. This is because the two classes of media are fundamentally different in how they function. Whereas protein retention in conventional media is modeled as adsorption at an extended two-dimensional surface, PDMs show a partitioning into the three-dimensional polymer phase [8]. Mechanistic understanding of protein mobility in these media is limited. Consequently, detailed mechanistic modeling of these materials is challenging, although it is vital not only to improve their performance, but also to allow predictive support for novel materials research and industrial process development. More experimental characterization can lead to more fundamental, protein-level understanding of the structure and dynamics of proteins in such media. Here we propose a novel method to measure protein adsorption in these chromatographic media with protein-scale resolution, namely small-angle neutron scattering.

### **1.3 Small-Angle Neutron Scattering**

Small-angle neutron scattering (SANS) is a well-established experimental technique based on the scattering of neutrons from structural heterogeneities [13]–[15]. SANS is a powerful technique to analyze the size, shape, structure, and interaction of complex systems with typical size ranging from a few nanometers up to tenths of a micrometer [13]. SANS is minimally disruptive and allows the study of both static and dynamic aspects of the structure [16]. As such, it is an appropriate

technique to study and characterize the protein mobility in PDMs on the length scales of interest, though it has never been used explicitly for this purpose previously.

In SANS experiments the intensity of neutrons is collected as a function of their deflection from the incident beam. The angle of this deflection is defined as  $2\theta$ , but typically SANS data are shown as a function of the momentum transfer vector or scattering vector  $Q$ , which is given by [15]

$$Q = \frac{4\pi}{\lambda} \sin \theta. \quad 1$$

In this equation,  $\lambda$  is the wavelength of the neutrons. The momentum transfer vector  $Q$  has dimensions of inverse length, *e.g.*  $\text{\AA}^{-1}$ , and experimental data given as a function of  $Q$  are therefore appropriately termed as being in inverse-space. It is directly related to the probed length scales  $L$  in real-space by introduction of the latter equation into the Bragg law [13], *i.e.*

$$L = \frac{2\pi}{Q}. \quad 2$$

Hence, experimental results from SANS experiments can be directly linked to real-space features in the sample.

The measured intensity  $I(Q)$  ( $\text{counts s}^{-1}$ ) is the measured count rate of neutrons at a certain deflection or momentum transfer  $Q$ . The measured intensity provides information about the sample structure at the probed length scales. As the measured count rate  $I(Q)$  is a function of the experimental set-up, the data are often reduced to an absolute scale, the scattering cross-section normalized to unit sample volume  $(d\Sigma/d\Omega)(Q)$  ( $\text{cm}^{-1}$ ). The relationship between the scattering cross-section and the measured count rate  $I(Q)$  in a detector element with area  $\Delta a$  and counting efficiency  $\varepsilon$ , situated normal to the scattered beam at a distance  $r$  from the sample, is given by

$$\left(\frac{d\Sigma}{d\Omega}\right)(Q) = \frac{I(Q)}{dT} \frac{r^2}{\varepsilon I_0 \Delta a A} = \frac{I(Q)r^2}{dT K_N A}. \quad 3$$

Here,  $I_0$  is the neutron flux (counts  $\text{s}^{-1}\text{cm}^{-2}$ ) on a sample area  $A$ , thickness  $d$  and volume  $V = Ad$ .  $K_N$  is a neutron calibration constant given by  $K_N = \varepsilon I_0 \Delta a$ . The measured transmission  $T$  is given by  $T = \exp(-\mu d)$ , where  $\mu$  is the linear attenuation coefficient of the beam on passing through the sample [17]. However, note that  $I(Q)$  is often used to represent the scattering spectrum in general, independent of units or reduction.

Neutron scattering is caused by a difference in scattering length density (SLD)  $\beta$  of the different phases in a heterogeneous system. More specifically, the intensity of deflected neutrons is proportional to the squared difference of the scattering length density between the phases, *i.e.* for a two-phase system

$$\left(\frac{d\Sigma}{d\Omega}\right)_{\text{coh}}(Q) \propto (\beta_1 - \beta_2)^2 = \Delta\beta^2, \quad 4$$

where  $\Delta\beta^2$  is called the contrast factor [14], [15]. The SLD of a material is dependent on its atomic composition. Interestingly, the SLD of isotopes can vary widely. Specifically, the coherent scattering length densities of  $\text{D}_2\text{O}$  and  $\text{H}_2\text{O}$  are  $6.33 \times 10^{-6} \text{ \AA}^{-2}$  and  $-5.60 \times 10^{-7} \text{ \AA}^{-2}$ , respectively [18]. This means that a  $\text{D}_2\text{O}:\text{H}_2\text{O}$  mixture can have an SLD anywhere between these values. As the SLD of most biological materials lies in this range, it is possible to prepare a  $\text{D}_2\text{O}:\text{H}_2\text{O}$  solution that matches one of the sample's phases in SLD. Consequently, this phase will not be detected by SANS measurements, making it virtually 'invisible'. This contrast variation or contrast matching technique is one of the most important advantages of SANS. It allows one to selectively probe certain phases in the sample by making one phase invisible. In theory, this can be applied to the study of protein adsorption on chromatographic resin particles by contrast matching out the particle matrix and

studying the structure of the adsorbed protein. This is an entirely novel way to study these systems.

#### **1.4 Thesis Objectives and Outline**

The application of SANS for the study of protein adsorption on chromatographic resin particles has, to the knowledge of the author, not been investigated before. The thesis describes a preliminary study to confirm the feasibility of the method and presents a framework and first results to promote the use of it. As such, the basis will be provided to acquire better experimental characterization of polymer-derivatized chromatographic materials, with the goal of stimulating the development of better mechanistic models in the future.

The use of contrast matching is a naturally attractive technique to study these systems. By contrast matching the PDM particle with the solvent, one would observe only the desired protein structures. However, PDM particles have a heterogeneous composition containing both a base matrix material and an attached polymer phase. Hence, the resulting system will, in principle, contain four distinct phases: the proteins, the solvent, the PDM base matrix, and the PDM attached polymer phase. Consequently, it would be impossible to fully match out the particles with the solvent. To solve this problem, the thesis studies the scattering from a cellulosic S HyperCel particle where both the base matrix and the attached polymer phase are composed of cellulose. This way, assuming that scattering from the relatively limited quantity of functional ligands can be neglected, one can fully contrast match the particle with the solvent. Cellulose is an often used base matrix material for chromatographic particles, and is comparable to other common materials like agarose [2], [3], [6], [19]–[21]. Though the investigated particles are, in essence, not polymer-derivatized, their gel-

like structure with functional ligands has been proposed to exhibit similar structural characteristics to the broader class of polymer-derivatized resins [19].

The thesis presents experimental data on two sets of SANS experiments, one without and one with protein adsorption on the chromatographic particles. The protein used for these studies is lysozyme. The experiment without protein adsorption is a typical contrast matching experiment; the experiment with protein adsorption investigates different protein loadings of the resin particles. From these experiments, the possible application of contrast matching is studied. However, the thesis shows that the basic contrast matching technique is not viable for this system, as the scattering length densities of cellulose and lysozyme (and thus most proteins in general) are too close together. Consequently, contrast matching of the particle will also lead to a high reduction of the contrast factor between the protein and the solvent, making data collection infeasible.

Instead, the thesis presents a framework to allow the quantitative study of protein adsorption in these systems without using contrast matching, by direct comparison of the scattering spectra with and without protein adsorption. To achieve this, the thesis derives a theoretical model for the scattering from the pure cellulosic resin particles, based on thermodynamic considerations and derivations from the literature. Furthermore, generally applicable methods are proposed to fully reduce the data to allow quantitative discussion of the results. The thesis shows that there is a clear change in the scattering spectrum upon protein adsorption. The origin of these changes is attributed to the presence of the protein by quantitative evidence from the sample compositions.



In Chapter 2, the sample preparation and set-up of the SANS experiments are specified. The sample compositions are shown in Chapter 3. This chapter also clarifies the methods by which the data are reduced to allow quantitative comparison between the samples and experiments: background removal and scaling of the scattering curves. Chapter 4 provides an explanation and derivation of the theoretical model for scattering from pure cellulosic resin particles. In Chapter 5, this model is used to quantify the change in scattering upon protein adsorption. The changes are explained in light of the physical picture of protein adsorption and compared to sample compositions to provide evidence for the proposed explanations. Finally, conclusions and suggestions for future work are included in Chapter 6.

## **Chapter 2**

### **EXPERIMENTAL METHODS**

This chapter provides detailed information on the methods and materials used in the experimental work. Two sets of SANS experiments were conducted for this thesis. The first experiment, named the contrast matching (CM) experiment, studies the resin particles without adsorbed protein. The second experiment, named the protein adsorption (PA) experiment, naturally studies the resin particles after protein adsorption. Section 2.1 gives an overview of the materials used, while Section 2.2 explains their use in the sample preparation. Section 2.3 contains the set-up of the SANS experiment.

#### **2.1 Materials**

##### **2.1.1 Buffers**

Monobasic sodium phosphate ( $\text{NaH}_2\text{PO}_4$ ), sodium chloride ( $\text{NaCl}$ ), and deuterium oxide ( $\text{D}_2\text{O}$ ) at 99.8 atom % D were purchased from Fisher Scientific (Fair Lawn, NJ). They were used to prepare 10 mM sodium phosphate buffer solutions in both deionized (DI) water ( $\text{H}_2\text{O}$ ) and  $\text{D}_2\text{O}$  at pH 7. The total ionic strength (TIS) in the  $\text{H}_2\text{O}$  solutions was adjusted using  $\text{NaCl}$  to 10 mM, 50 mM, and 100 mM TIS. In addition, deuterium oxide ( $\text{D}_2\text{O}$ ) was used to create unbuffered 20 mM, 100 mM, and 200 mM TIS solutions by addition of  $\text{NaCl}$ .

### **2.1.2 Protein solutions**

Hen egg white lysozyme (molecular weight [MW] 14.3 kD) was purchased from Sigma-Aldrich. Solutions were prepared by dissolving lyophilized protein in the desired TIS-controlled buffer and concentrated using 10K Amicon centrifugal filters. Concentrated samples were rediluted with buffer and reconcentrated three times for the 10 mM TIS solution and twice for the 50 mM and 100 mM TIS solutions. Protein concentrations were determined using UV spectrophotometry (a Shimadzu UV-1700 and a Thermo Scientific NanoDrop 2000). Protein concentrations in stock solutions were 108.2 mg/mL for the 10 mM TIS solution, 100.7 mg/mL for the 50 mM TIS solution, and 115.0 mg/mL for the 100 mM TIS solution.

### **2.1.3 Stationary phase**

S HyperCel (lot AU31072012-4) was provided by Pall Corporation (Northborough, MA). The resin is synthesized from a cellulosic base matrix with a sulfonate ligand for cationic exchange (CEX). The average particle size is on the order of 75 – 80  $\mu\text{m}$ . The resin was washed three times by subsequent addition of DI  $\text{H}_2\text{O}$  and centrifuging and decanting the solution. This was followed by solvent exchange with  $\text{D}_2\text{O}$  by repeating this procedure twice with the appropriate  $\text{D}_2\text{O}$  solution and letting the solution equilibrate in a twelve-hour interval.

## **2.2 Sample Preparation**

### **2.2.1 Contrast matching experiment**

A series of 10 mM TIS buffer solutions were prepared in  $\text{D}_2\text{O}$ :  $\text{H}_2\text{O}$  fractions of 0 mole %, 20 mole %, 50 mole %, 75 mole %, and 100 mole %. Samples were

prepared by letting 0.5 mL hydrated particle volume (hpv) of resin equilibrate with these solutions.

### 2.2.2 Protein adsorption experiment

A series of samples was prepared for different TIS conditions and protein concentrations. Each sample was prepared with (1) 0.5 mL hydrated particle volume (hpv) of resin equilibrated with pure D<sub>2</sub>O, (2) a certain volume of protein solution determined by the desired final protein concentration, and (3) D<sub>2</sub>O solution to bring the total sample volume to 10 mL. Samples for neutron scattering experiments were prepared in D<sub>2</sub>O instead of H<sub>2</sub>O because of the high contrast for the hydrogenous sample in D<sub>2</sub>O. The 10 mM, 50 mM, and 100 mM TIS protein solutions were combined with the 20 mM, 100 mM, and 200 mM TIS D<sub>2</sub>O solutions, respectively. This mismatch was due to a mistake during D<sub>2</sub>O solution preparation. As the D<sub>2</sub>O solutions are not buffered, the pH of these samples is not controlled.

Samples were allowed to reach protein adsorption equilibrium by rotation over a 48-hour period, after which protein concentrations in the supernatant solutions were determined for each sample using UV spectrophotometry (a Shimadzu UV-1700 and a Thermo Scientific NanoDrop 2000).

The amount adsorbed at the end of each experiment  $q$  (mg/mL hpv) was determined by mass balance

$$q = \frac{V}{V_m} (C_0 - C) \quad 5$$

where  $V$  (mL) is the total solution volume,  $V_m$  (mL hpv) is the hydrated particle volume (hpv),  $C_0$  (mg/mL) is the initial protein concentration, and  $C$  (mg/mL) is the final protein concentration in the supernatant.

## 2.3 Small-Angle Neutron Scattering

### 2.3.1 Contrast matching experiment

The experiment was carried out on the 30 m NG7 SANS instrument at the National Center for Neutron Research (NCNR), National Institute of Standards and Technology (NIST), Gaithersburg (MD). The tests were run in three configurations:

- high- $Q$ : 1 m sample-to-detector distance (SDD) with 6 Å neutrons for a 360 s count time,
- intermediate- $Q$ : 4 m SDD with 6 Å neutrons for 600 s count time, and
- low- $Q$ : 15.3 m SDD with lenses with 8 Å neutrons for a 900 s count time,

yielding a scattering variable range between  $0.0009 \text{ Å}^{-1} < Q < 0.5 \text{ Å}^{-1}$ . Standard data reduction procedures were followed using the program IGOR Pro in order to obtain corrected and radially averaged SANS macroscopic scattering cross-sections [22]. Demountable quartz window sample cells with a path length (thickness)  $d$  of 1 mm were used for all samples.

### 2.3.2 Protein adsorption experiment

The experiment was carried out on the 30 m NG3 SANS instrument at NCNR, NIST. The tests were run at a:

- high- $Q$ : 1 m SDD with 6 Å neutrons for a 360 s count time,
- intermediate- $Q$ : 4 m SDD with 6 Å neutrons for 600 s count time, and
- low- $Q$ : 13 m SDD with lenses with 8 Å neutrons for a 900 s count time,

yielding a scattering variable range between  $0.001 \text{ \AA}^{-1} < Q < 0.4 \text{ \AA}^{-1}$ . Standard data reduction procedures were followed using the program IGOR Pro in order to obtain corrected and radially averaged SANS macroscopic scattering cross-sections [22]. Demountable quartz window sample cells with a path length (thickness)  $d$  of 1 mm were used for all samples.

## Chapter 3

### DATA ACQUISITION AND REDUCTION

This chapter explains the several steps in the data reduction process. Firstly, in Section 3.1 it provides the sample compositions of the several samples used. Then, Section 3.2 presents the SANS spectra after basic reduction. Further reduction is achieved in Sections 3.3 and 3.4, which deal with removal of the incoherent background and scaling of the spectra, respectively.

#### 3.1 Sample Compositions

Five samples, labeled A to E, were prepared for the contrast matching (CM) experiment with a  $D_2O:H_2O$  fraction ranging from 0 mole % to 100 mole %. Table 1 gives an overview of these samples.

Table 1: Overview of the contrast match samples.

Sample	$D_2O:H_2O$ fraction [mole %]
A	0
B	20
C	50
D	75
E	100
11	100

Table 2: Overview of adsorption values in the protein adsorption experiments.

Sample	TIS [mM]	$C_0$ [mg/mL]	$C$ [mg/mL]	$q$ [mg/mL hpv]
1	35.2	14.1	8.6	109.7
2	34.8	16.2	10.6	112.8
3	34.3	18.4	12.4	120.7
4	33.5	22.7	17.6	102.7
5	88.8	11.6	6.3	105.2
6	84.5	19.6	14.4	104.6
7	186.5	3.7	0.6	60.9
8	183.7	6.7	2.6	81.6
9	181.8	8.7	4.2	91.8
10	173.0	18.1	9.5	170.8
F	10.0	11.6	0.32	224.9

Ten samples, labeled 1 to 10, were prepared for the protein adsorption (PA) experiment. The samples were prepared at three different total ionic strengths (TIS) of 40 mM, 100 mM, and 200 mM. However, the TIS of the initial protein solutions was half of these values and the resin slurry was prepared in pure D<sub>2</sub>O. Hence, the actual TIS of the samples, shown in Table 2, is slightly lower than these target values (about 10%).

The ten PA samples also differ in initial protein concentration  $C_0$ , ranging from 3.68 g/mL to 22.7 g/mL. These values, along with the measured final protein concentration in the supernatant after equilibrium  $C$ , are included in Table 2. They allow for the calculation of the adsorbed protein concentration  $q$  via Equation 5 (page 12). The result is illustrated in Figure 1, and in general resembles a typical set of protein adsorption isotherms as a function of TIS, for which one would expect that the isotherm decreases with increasing TIS [20]. An exception to this trend is sample 10, which reflects a high level of adsorption at high TIS and therefore seems to be an



outlier. The reason for this high adsorption is unknown. In addition to this discrepancy, isotherms for this system have been shown to exhibit greater adsorption  $q$  than measured here [20]. The lower adsorption might be due to several factors, including the lack of pH control and  $D_2O$  being the solvent instead of  $H_2O$ . The overlap of the isotherms might be caused by the same factors, in addition to the general tendency that the isotherms approach each other at higher TIS.

The composition of the PA samples after adsorption is given in Table 3. For these calculations, it was assumed that (1) the solution containing  $D_2O$ ,  $H_2O$ , unadsorbed protein, and NaCl is uniform throughout the sample; and (2) the adsorbed protein replaces the solution inside the particle, without decreasing the cellulose content per hydrated particle volume. The cellulose content is calculated from the known volume of cellulosic particles per hydrated particle volume and the cellulose density. From this, the sulfonate ligand content can be calculated from the known ligand density, as reported by the manufacturer. Note that the amount of  $H_2O$  in the samples introduced by the initial protein solution is definitely significant.

One extra sample was prepared for both the CM and PA experiment. For the CM experiment, a sample was prepared in which protein is adsorbed in a 100 mole %  $D_2O$  solution. This sample is labeled sample F in Table 2. For the PA experiment, a sample was prepared without the adsorption of protein. This sample is labeled sample 11 in Table 1. By design, these samples provide assurance that the two sets of experiments – performed on two different SANS instruments – are compatible. However, these samples are not used in the data interpretation.

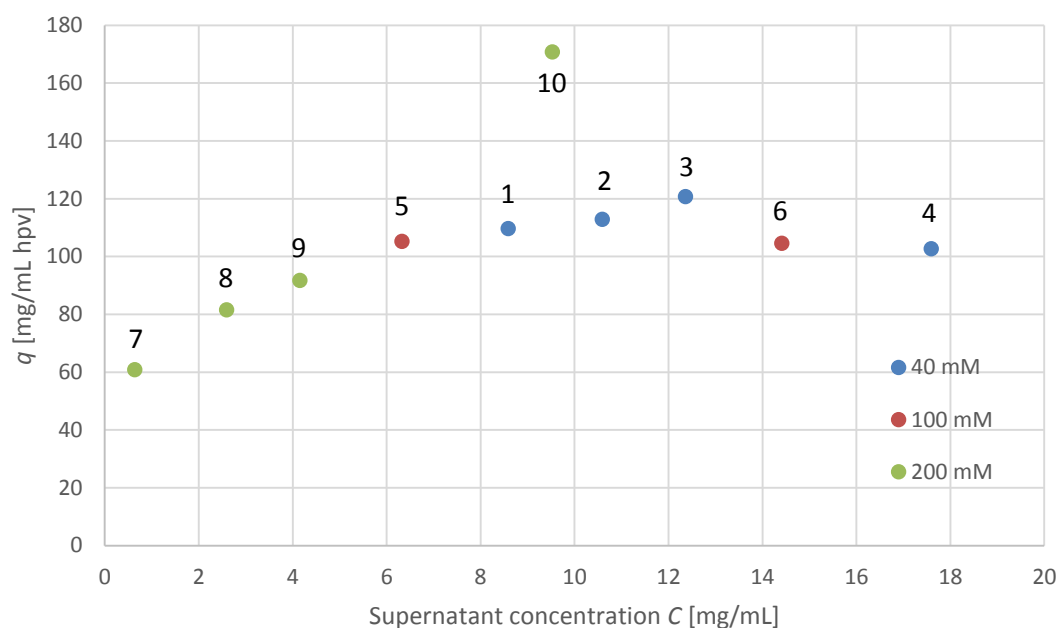


Figure 1: Adsorbed amounts in the protein adsorption samples as a function of supernatant concentration. The TIS values shown are approximate. Sample numbers are indicated.

Table 3: Detailed protein adsorption sample compositions.

Sample	Composition [g/mL hpv]						
	Cellulose	Sulfonate	D <sub>2</sub> O	H <sub>2</sub> O	NaCl	Protein	
						Adsorbed	In solution
1	0.259	0.00706	0.733	0.101	0.00171	0.110	0.0072
2	0.259	0.00706	0.715	0.117	0.00169	0.113	0.0088
3	0.259	0.00706	0.694	0.132	0.00166	0.121	0.0102
4	0.259	0.00706	0.673	0.166	0.00164	0.103	0.0148
5	0.259	0.00706	0.747	0.090	0.00435	0.105	0.0053
6	0.259	0.00706	0.683	0.154	0.00414	0.105	0.0121
7	0.259	0.00706	0.844	0.026	0.00948	0.061	0.0006
8	0.259	0.00706	0.809	0.046	0.00917	0.082	0.0022
9	0.259	0.00706	0.787	0.060	0.00900	0.092	0.0035
10	0.259	0.00706	0.674	0.115	0.00798	0.171	0.0075

### 3.2 Small-Angle Neutron Scattering Spectra

Standard data reduction procedures were followed using the program IGOR Pro in order to obtain corrected and radially averaged SANS macroscopic scattering cross-sections from the raw experimental data [22]. Consequently, the depicted scattering intensities are on an absolute scale, *i.e.* they are the differential scattering cross-section  $(d\Sigma/d\Omega)(Q)$ . The result is shown in Figure 2 for the CM samples and Figure 3 for the PA samples. All the data show a monotonically decreasing profile as a function of scattering vector  $Q$ . The figures include an indication of the real-space length scales that correspond to the scattering features as calculated by Equation 2 (page 5,  $L = 2\pi/Q$ ).

Due to problems during loading of the sample into the sample cell, no scattering spectrum was obtained for samples 2 and 3. In addition, a big air bubble was observed in the sample cell of sample 10 after the scattering experiment, rendering the scattering spectrum for this sample unreliable. This is unfortunate, as sample 10 was an outlier during sample preparation, and study of this sample would have been interesting.

Note that the two consistency samples, sample F and sample 11, correspond well to the other samples. Hence, we can conclude that the two experiments are indeed consistent, and that we can use them together in data analysis.

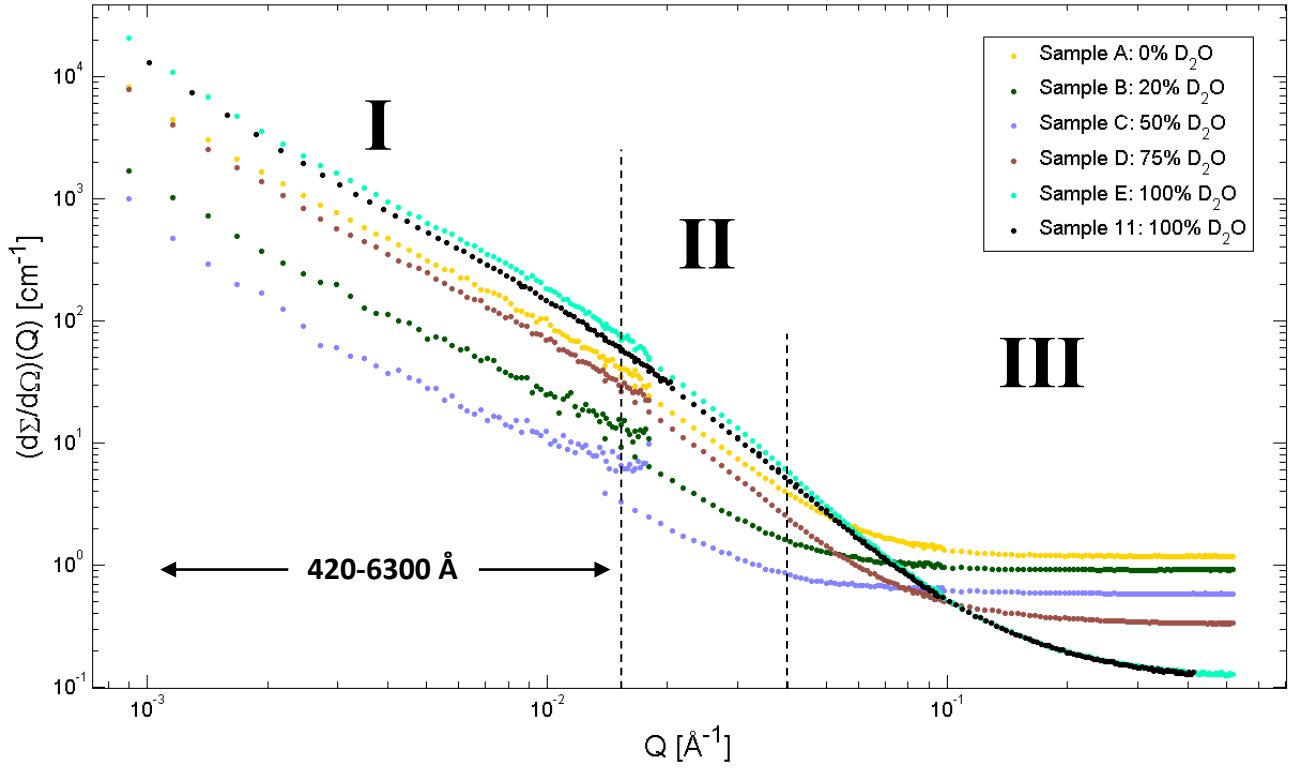


Figure 2: Scattering spectra after basic reduction for the contrast matching samples.

### 3.3 Removal of the Incoherent Background

The differential scattering cross-section consists of differential coherent and incoherent scattering cross-sections [23]:

$$\left(\frac{d\Sigma}{d\Omega}\right)(Q) = \left(\frac{d\Sigma}{d\Omega}\right)_{\text{coh}}(Q) + \left(\frac{d\Sigma}{d\Omega}\right)_{\text{inc}}. \quad 6$$

Unlike the coherent scattering cross-section, the incoherent scattering cross-section provides no information on structure and is unnecessary background. It originates mainly from the large incoherent scattering cross-section of the H atom. Since the composition of the samples is different, so is the incoherent background. Hence, the subtraction of incoherent scattering is one of the important procedures in data reduction of SANS data and quantitative analysis.

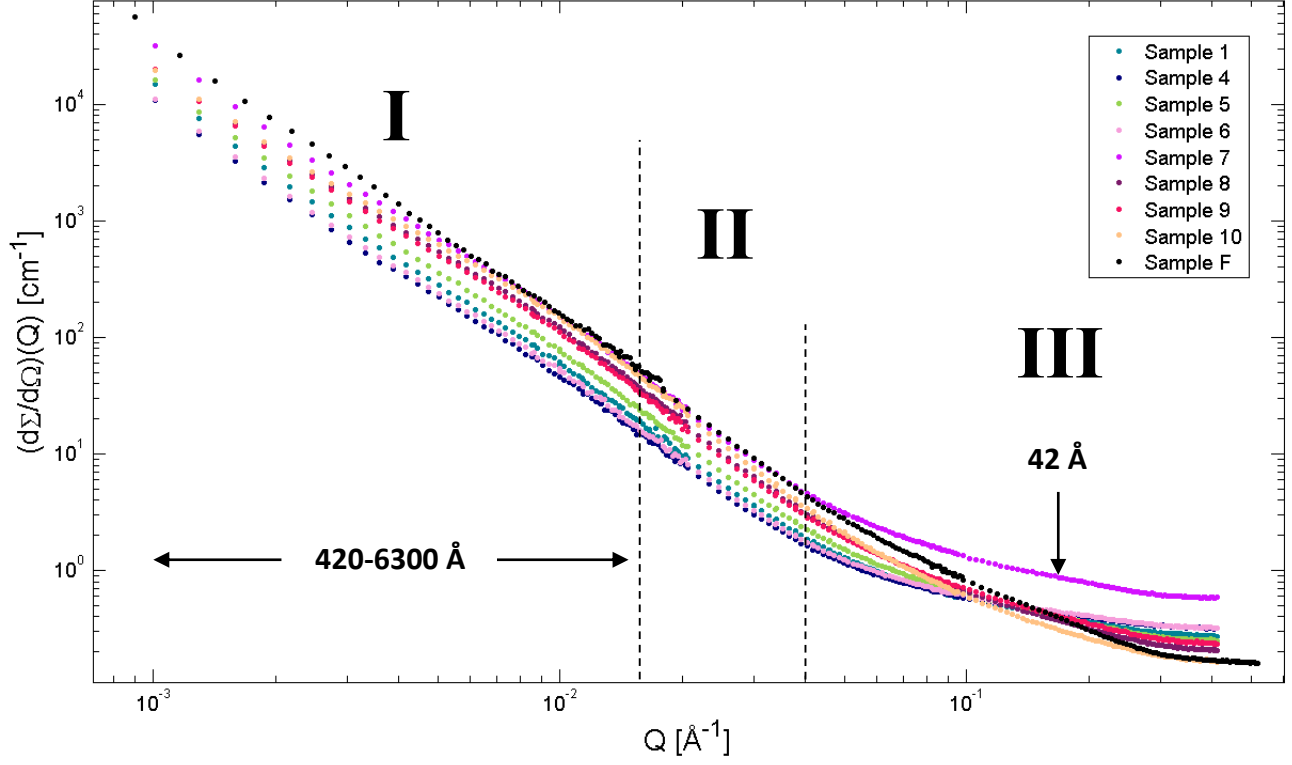


Figure 3: Scattering spectra after basic reduction for the protein adsorption samples.

The observed experimental background can easily be determined via the Porod law [14]. This law states that in the high- $Q$  regime, the coherent scattering intensity is proportional to  $Q^{-4}$ , *i.e.*

$$\left(\frac{d\Sigma}{d\Omega}\right)(Q) = \frac{A}{Q^4} + B \quad 7$$

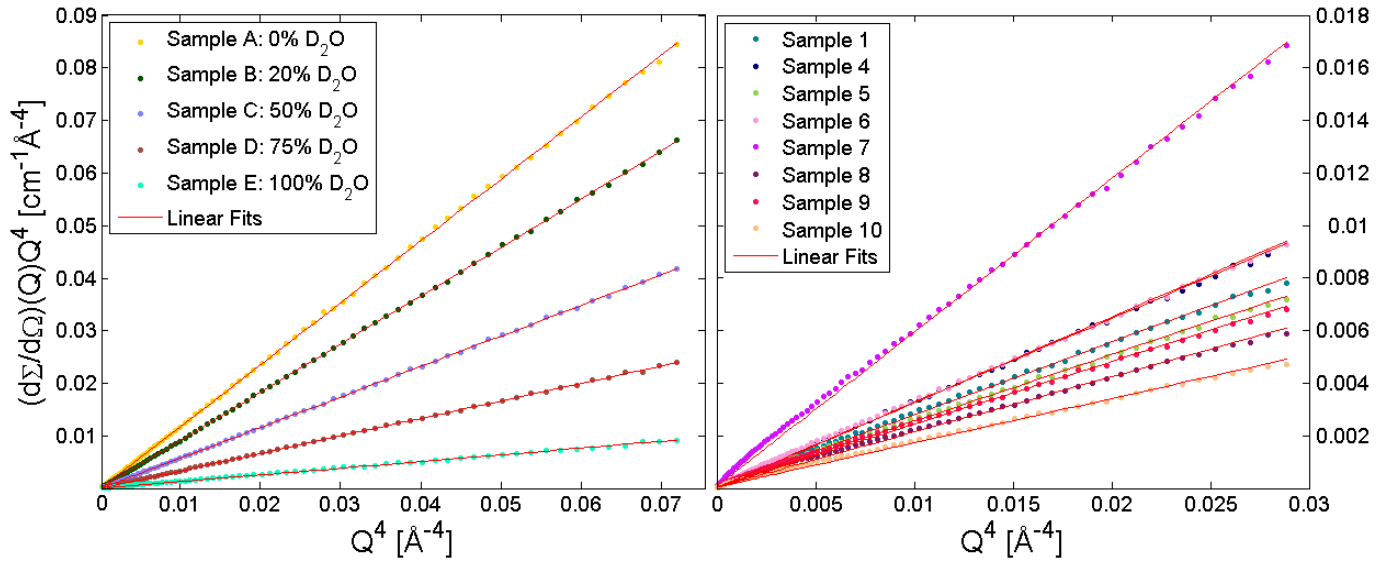


Figure 4: Porod plots for the contrast matching samples (left) and protein adsorption samples (right). The incoherent background  $B$  can be determined from the slope of the linear fit (red).

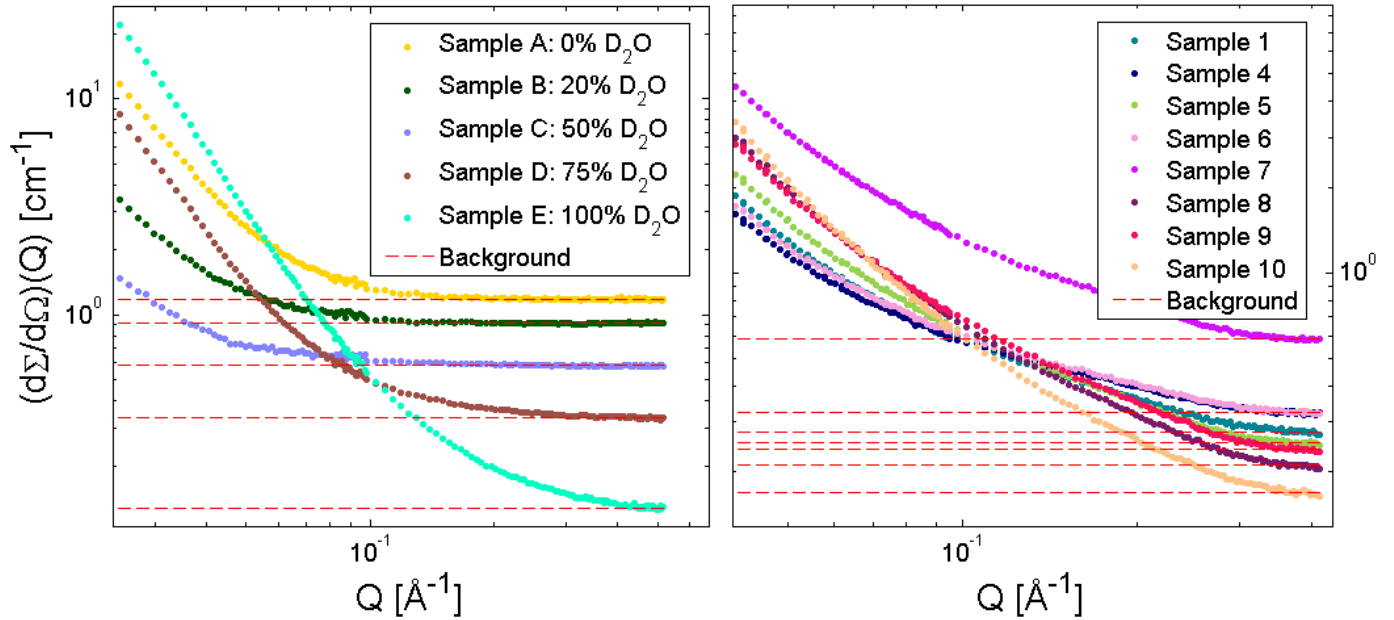


Figure 5: Illustration of the experimentally determined background values of the scattering spectra for the contrast matching samples (left) and protein adsorption samples (right).

In this equation,  $A$  is a constant and  $B = (d\Sigma/d\Omega)_{\text{inc}}$  denotes the incoherent background scattering. This means that the background can be obtained directly from the slope in a linear plot of  $(d\Sigma/d\Omega)(Q) \cdot Q^4$  vs.  $Q^4$ . These so-called Porod plots are shown in Figure 4 for the CM and PA experiments. Indeed, the plots show straight lines in the high- $Q$  regime. The acquired values for the background are gathered in Table 4. Figure 5 displays these background values on the scattering spectra.

Subtraction of this background contribution from the differential scattering cross-section provides the differential coherent cross-section (Equation 6). Figure 6 depicts the scattering spectra after removal of the incoherent background. Since the data are represented on a logarithmic plot, all spectra have been given the same background value  $B_0$  for clarity. The chosen value for  $B_0$  of  $0.13 \text{ cm}^{-1}$  is the background from the pure resin in 100 mole %  $\text{D}_2\text{O}$  (sample E and sample 11).

### 3.4 Scaling of the Spectra

#### 3.4.1 Contrast matching experiment

The scattering intensity is dependent on the scattering length density (SLD) contrast between the phases in the sample. More specifically, for a two-phase system, we know that the coherent scattering spectrum scales with the scattering length density difference squared or contrast factor (Equation 4 on page 6), *i.e.*

$$\left(\frac{d\Sigma}{d\Omega}\right)_{\text{coh}}(Q) \propto (\beta_p - \beta_s)^2 = \Delta\beta^2,$$

where  $\beta_p$  and  $\beta_s$  are the SLD of the resin particles and solution, respectively [14], [15]. When sample compositions are identical except for the  $\text{D}_2\text{O}:\text{H}_2\text{O}$  fraction in the solution, we expect the scattering spectra to overlap after scaling by this factor. Hence,

Table 4: Experimentally determined, incoherent background values from the Porod plot.

	CM experiment						PA experiment								
Sample	A	B	C	D	E	F	1	4	5	6	7	8	9	10	11
Background $B$ [ $\text{cm}^{-1}$ ]	1.18	0.92	0.58	0.33	0.13	0.16	0.28	0.32	0.25	0.32	0.59	0.21	0.24	0.17	0.13

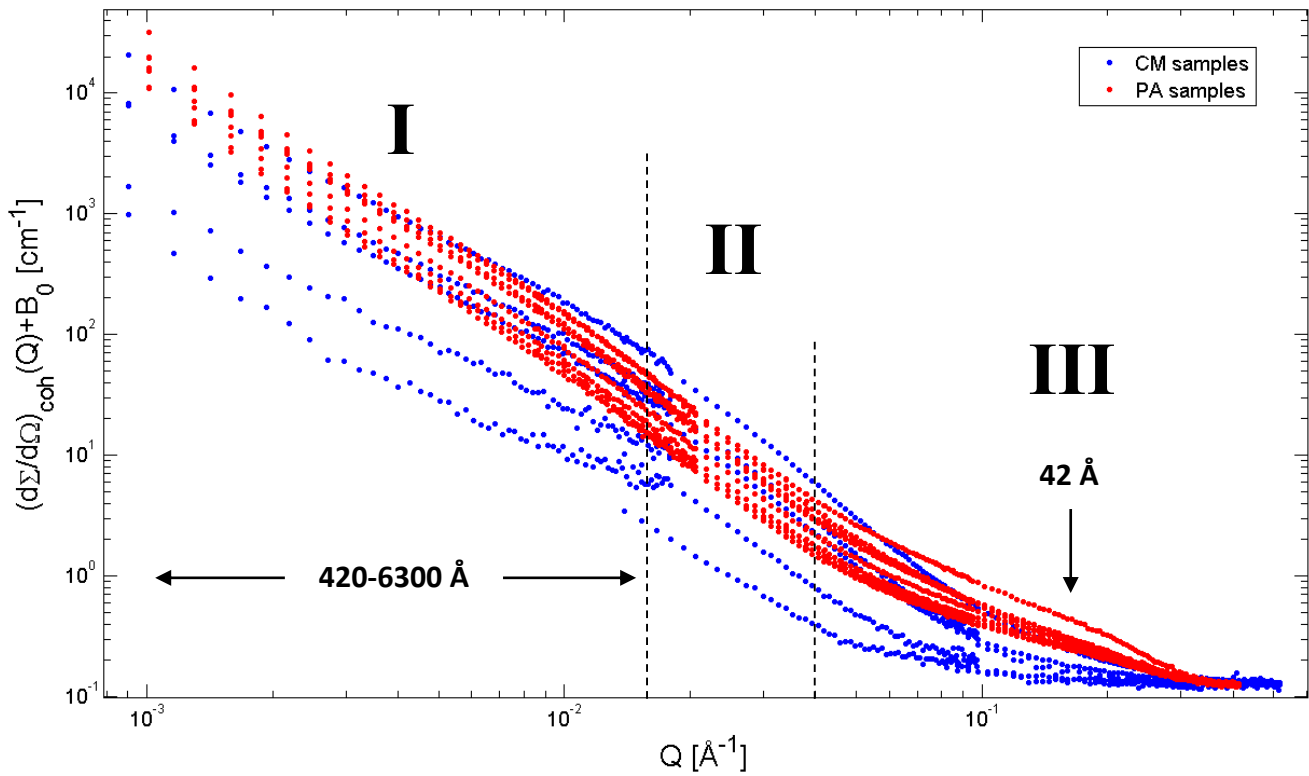


Figure 6: Scattering spectra after subtraction of the incoherent background. For display clarity, all spectra have been given the same background value.



we can define a scaling factor  $S = \Delta\beta^2$  which, after division, makes the scaling spectra overlap. The experimental scaling factor  $S$  for the different spectra has been determined via least squares fitting. The spectra are scaled relative to the scattering spectrum of sample E (pure resin in 100% D<sub>2</sub>O), making the scattering factor for sample E  $S_E = 1$  per construction. The experimentally obtained scattering factors are given in Table 5. The scaled spectra are shown in Figure 7.

The scattering length density of the resin particles is constant for all the samples. The scattering length density of the solution is a linear function of the D<sub>2</sub>O: H<sub>2</sub>O fraction  $f_{D_2O}$ ,

$$\beta_s = f_{D_2O} \cdot \beta_{D_2O} + (1 - f_{D_2O}) \cdot \beta_{H_2O}. \quad 8$$

The scattering length densities of D<sub>2</sub>O and H<sub>2</sub>O are  $6.33 \times 10^{-6} \text{ \AA}^{-2}$  and  $-5.60 \times 10^{-7} \text{ \AA}^{-2}$ , respectively [18]. Combination of Equation 4 and Equation 8 shows that the square root of the scaling factor  $\sqrt{S}$  depends linearly on the D<sub>2</sub>O: H<sub>2</sub>O fraction of the sample. In addition, from the D<sub>2</sub>O: H<sub>2</sub>O fraction at which  $\sqrt{S}$  becomes zero, and hence where the scattering spectrum virtually disappears, we can calculate the scattering length density of the resin particles. This is the so-called contrast match point (CMP). This is illustrated in Figure 8. The acquired CMP is around 38 mole % D<sub>2</sub>O, leading to an SLD for the resin particles of  $2.06 \times 10^{-6} \text{ \AA}^{-2}$ . This is comparable to SLD values for cellulose found in the literature [24], where SLD values for pure cellulose of  $1.86 \times 10^{-6} \text{ \AA}^{-2}$  (CMP 35 mole %) [25] and  $1.74 \times 10^{-6} \text{ \AA}^{-2}$  (CMP 33 mole %) [26] have been reported. The relatively small difference might be attributed to the presence of the sulfonate ligands and the fact that the cross-linked particles can differ slightly from pure cellulose in composition.

Table 5: Experimentally obtained scaling factors for the contrast matching samples, relative to sample E.

Sample	A	B	C	D	E
$S [-]$	0.409	0.088	0.046	0.378	1.000

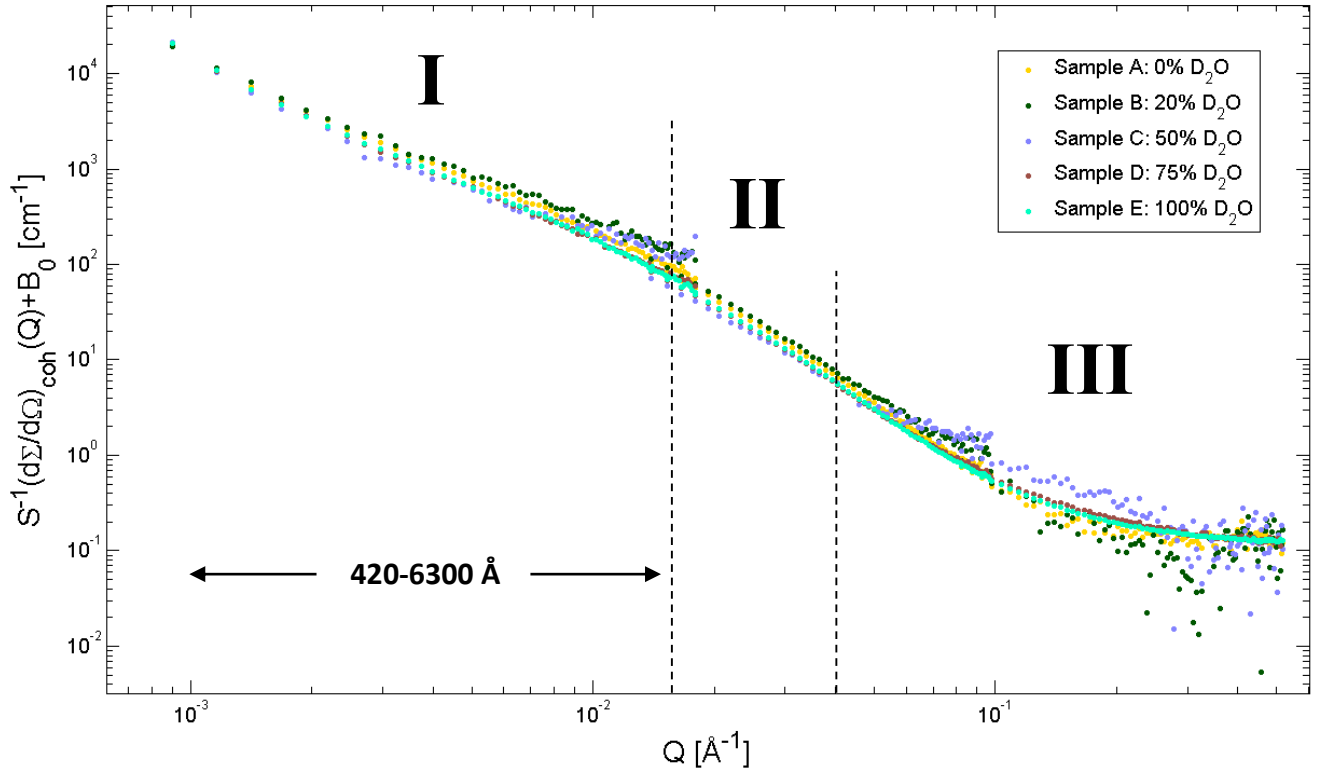


Figure 7: Scaled scattering spectra for the contrast matching experiment.

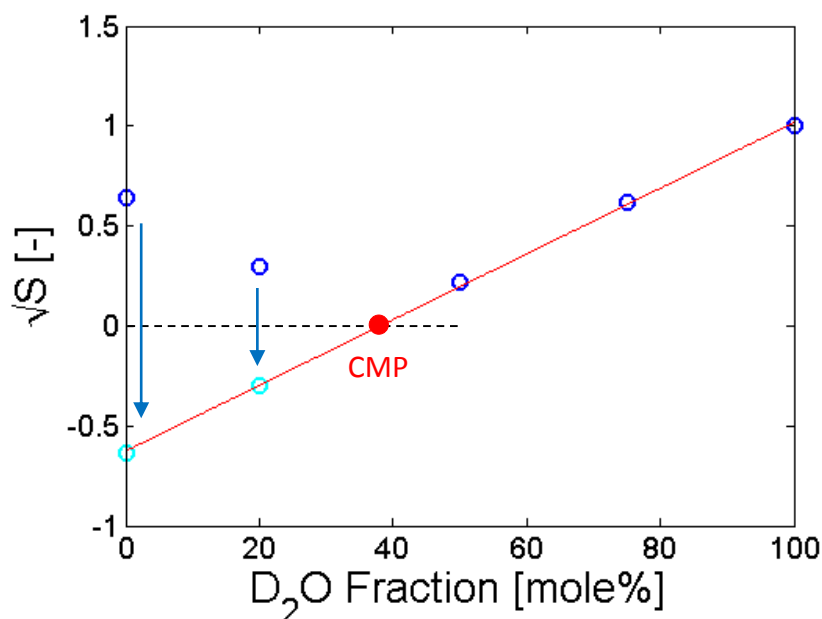


Figure 8: Square root of the scaling factors as a function of the D<sub>2</sub>O: H<sub>2</sub>O fraction in the sample solution (blue). To get a linear fit (red), some points have to be inverted to take the sign into account. The contrast match point (CMP) is found where the scaling factor is zero.

### 3.4.2 Protein adsorption experiment

As the composition of the protein adsorption samples varies, the scattering spectra will differ by more than just a scaling factor and they are not expected to overlap completely after scaling. Hence, the technique used for the contrast matching experiments to determine the scaling factors cannot be applied here. However, Equation 4 still applies, and the scaling should be accounted for to allow quantitative comparison between the scattering spectra of the samples.

To determine the scaling factors from the experimental data, it is necessary to scale the curves in a  $Q$ -range in which there are no structural changes due to the different sample compositions. The protein adsorption samples basically differ only in

protein loading. Consequently, one could expect to find a region where the protein concentration has no effect on the scattering curve. As can be seen in Figure 6 (page 24), the scattering curves are all parallel in the intermediate  $Q$ -regime, indicating that this region is dominated only by scattering from the resin particles. This is further elaborated upon in Section 5.1. Figure 9 confirms that the spectra in the intermediate- $Q$  region ( $0.02 \leq Q \leq 0.03$ ) are parallel, except for a deviation in sample 10, which is assumed to be an outlier. The linear fits in this figure are used to obtain the scaling factors.

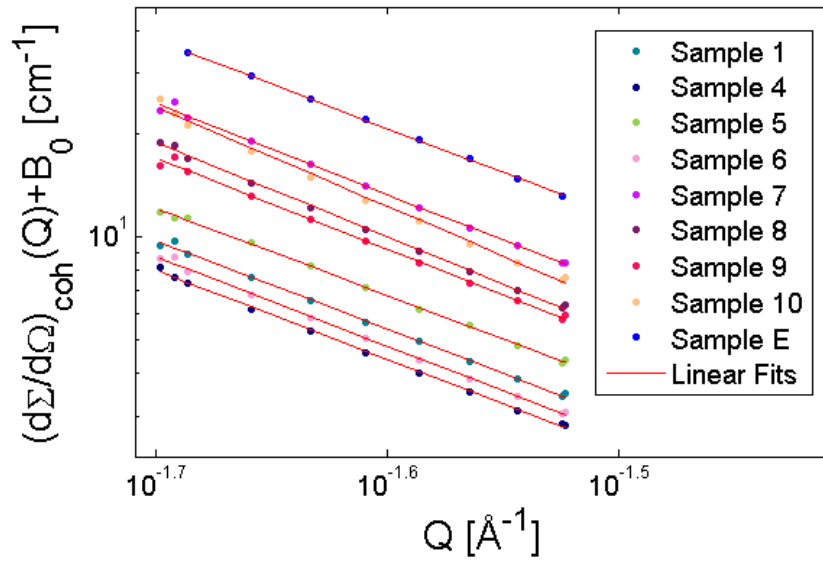


Figure 9: Illustration of how the scattering spectra are parallel and linear in the intermediate- $Q$  region ( $0.02 \leq Q \leq 0.03$ ).

The experimentally determined scaling factors  $S$  from the intermediate  $Q$ -regime are given in Table 6. The spectra are scaled relative to the scattering spectrum of sample E (pure resin in 100% D<sub>2</sub>O). The scaled spectra are shown in Figure 10.

Table 6: Experimentally obtained scaling factors for the protein adsorption samples, relative to sample E.

Sample	1	4	5	6	7	8	9	10
$S$ [–]	0.260	0.213	0.325	0.232	0.645	0.490	0.447	0.609

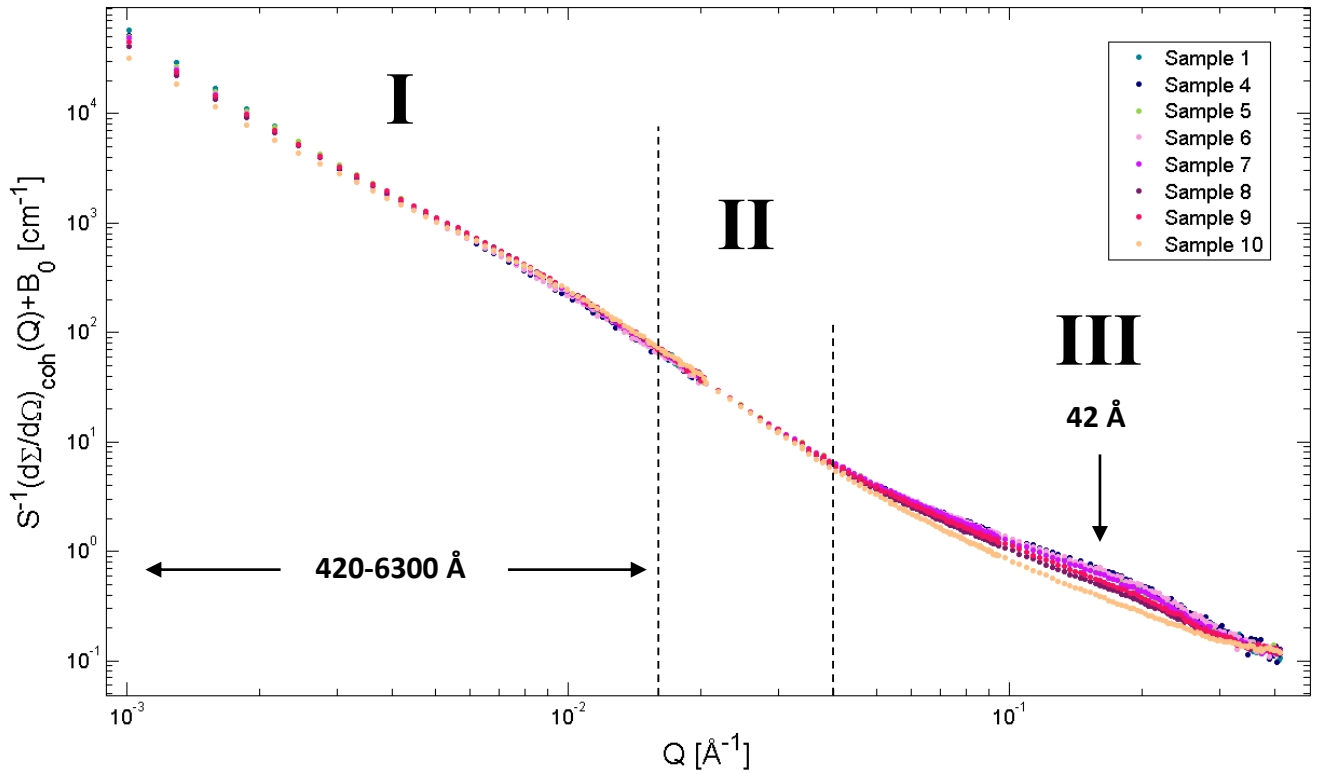


Figure 10: Scaled scattering spectra for the protein adsorption experiment.

## Chapter 4

### PARTICLE MODELING

This chapter is centered on creating a model to describe the scattering spectrum from the pure resin particles. Section 4.1 elaborates on the reasons that such a model is useful. In Section 4.2, an actual model is constructed from thermodynamic considerations and derivations from the literature. This model is compared to the generalized Guinier-Porod model in Section 4.3.

#### 4.1 Introduction

A fundamental goal of this thesis is to characterize the differences in scattering spectra between the particles before and after protein adsorption. From this difference, the adsorption mechanics and structure might be studied. A great advantage of SANS is the possibility to use the contrast matching technique. As shown in Equation 4 (page 6), the amount of scattering in a SANS experiment is determined by the contrast between the different phases in the system. In addition, due to the large difference in the scattering length density (SLD) of protonated and deuterated water ( $6.33 \times 10^{-6} \text{ \AA}^{-2}$  and  $-5.60 \times 10^{-7} \text{ \AA}^{-2}$ , respectively [18]), it is possible to prepare solutions with an SLD anywhere in this large range. Combination of these two factors allows the use of a solvent that identically matches the SLD of one of the phases in the system, making this phase basically invisible for neutron scattering techniques.

In theory, contrast matching of the cellulosic resin particles offers a way to study the structure of the adsorbed protein alone, without interference from the particles' scattering. However, using contrast matching of the resin particles to reveal the scattering spectrum of the adsorbed protein is difficult due to the similar scattering

length densities (SLDs). The scattering length density of the resin particles was shown in Chapter 3 to be  $2.06 \times 10^{-6} \text{ \AA}^{-2}$ , which corresponds to a contrast match point (CMP) of 38 mole %  $\text{D}_2\text{O}$ . In comparison, the SLD of lysozyme is calculated to be  $1.94 \times 10^{-6} \text{ \AA}^{-2}$  for a 0 mole %  $\text{D}_2\text{O}$  solution and  $2.56 \times 10^{-6} \text{ \AA}^{-2}$  for a 38 mole %  $\text{D}_2\text{O}$  solution, assuming 100% exchange of exchangeable hydrogens in the protein [27]. Contrast matching of the resin particles would automatically lead to a large reduction in contrast between the protein and the solvent, leading to a smaller scattering intensity and much longer beam exposure times.

Instead of using contrast matching, we propose to directly compare the scattering spectra before and after protein adsorption. Assuming that the resin particle scattering – and hence the particle structure – remains unchanged during adsorption, the change in the scattering spectra can be fully attributed to the presence of the protein. To characterize the scattering of the protein, it is necessary to model the scattering without adsorption of the protein, *i.e.* the scattering from the pure resin particles. The experimentally obtained scattering spectrum from the pure particles in 100 mole %  $\text{D}_2\text{O}$  (sample E) is used to derive a model for the scattering by the cellulosic particles.

The SANS spectrum of sample E is shown in Figure 11. The spectrum is qualitatively similar to spectra observed in polymer gel systems. Although no literature has been found on cellulose gels, several studies have been reported on agarose [16], [28] and other polymer gels [29]–[34]. These gels typically show fractal spectra. A schematic diagram of the spectrum for normal polymer gels is shown in Figure 12 [16]. As indicated by the figure, the spectrum can be divided into three regions. Those regions are clearly observed in the experimental data in Figure 11.

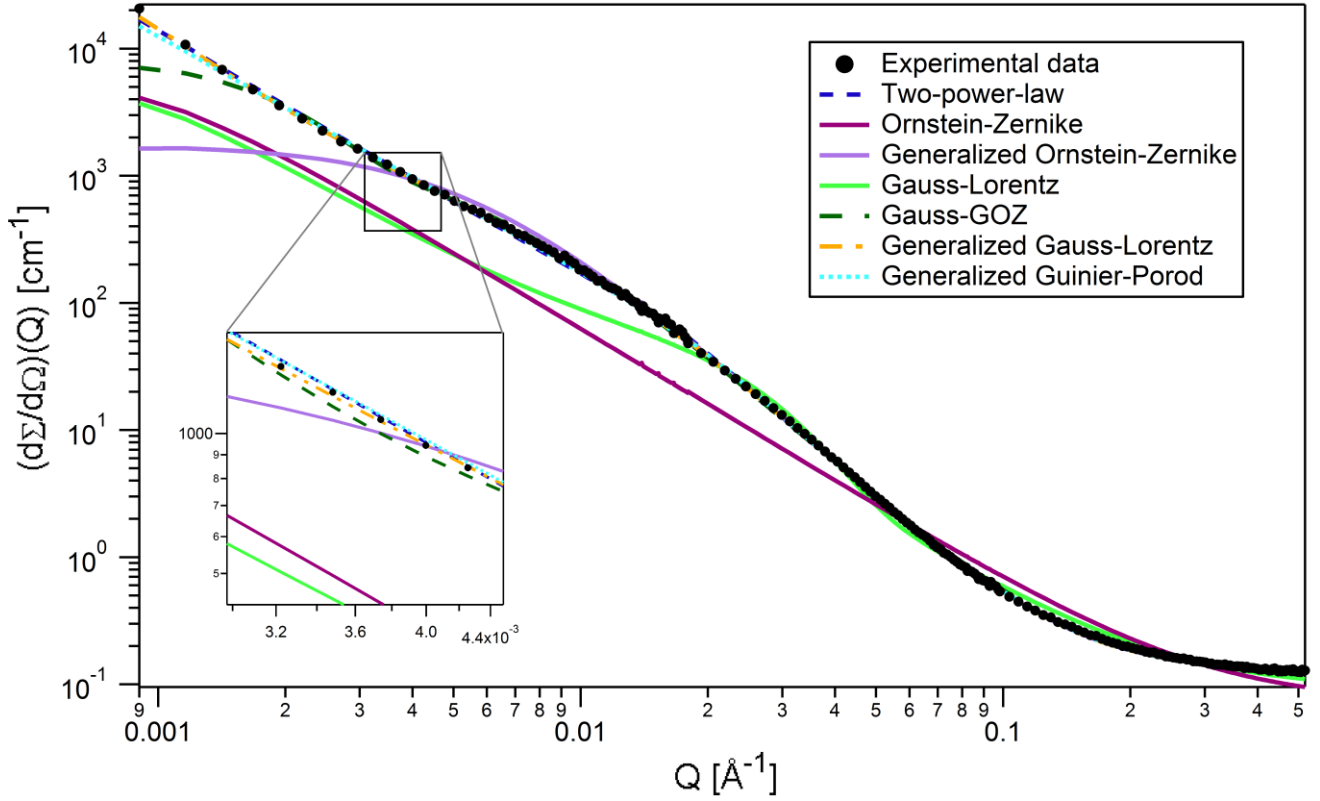


Figure 11: Illustration of how different models fit the SANS experimental data of cellulosic resin particles in deuterated water (sample E). The models are described in the text. Note that the Ornstein-Zernike and generalized Ornstein-Zernike models are fit only to the intermediate- and high- $Q$  regions ( $Q > 0.017 \text{ \AA}^{-1}$ ). All model parameters are kept adjustable for these fits.

The  $Q$ -ranges of the regions, and hence the corresponding length scales, agree very well with those observed in agarose [28]. The spectrum is continuous and smooth without maxima. The lack of a maximum, which corresponds to a lack of a correlation length, is likely due to polydispersity of pore and cluster sizes in the particle. The continuous increase at low  $Q$  is indicative of the cross-linking in the particle [28]. At



high  $Q$ , scattering is largely incoherent, probably due to hydrogen bound to the cellulose itself [16], [28].

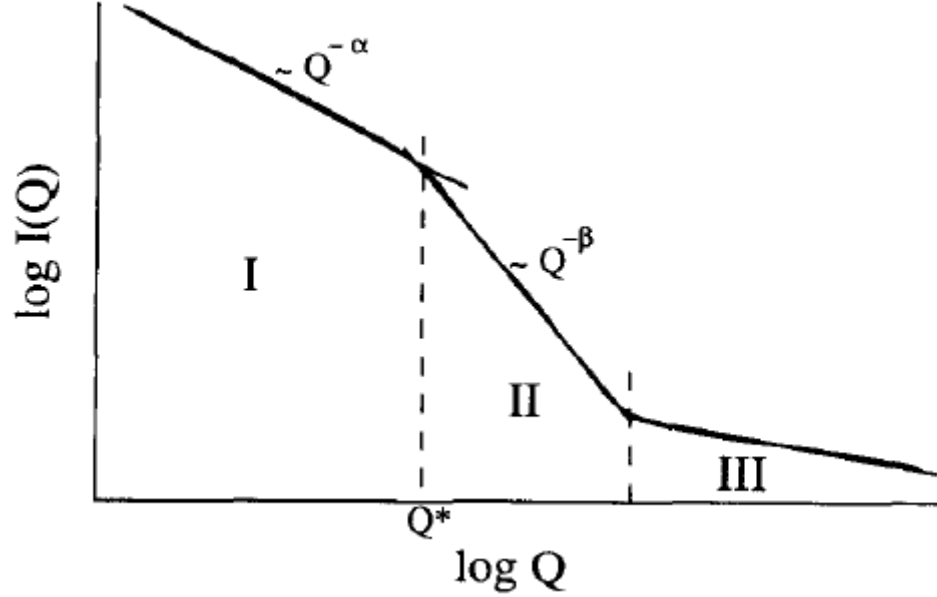


Figure 12: Schematic diagram of the spectrum for normal polymer gels [16].

#### 4.2 Model Construction

An obvious choice of model for this kind of spectrum would be a two-power-law model [35], [36]. Indeed, Figure 11 illustrates that the model fits the experimental data well. The slopes for the low- $Q$  and intermediate- $Q$  region are  $\alpha = 1.88$  and  $\beta = 2.82$ , respectively. These exponents are higher than those observed for agarose, indicating that the clusters in the cellulose particles are denser than to those in the agarose gels, which are statistical gels [28], [37].

The exact solution for the scattering function,  $I(Q)$ , has not yet been obtained for cross-linked polymer gels, because local fluctuations of fiber density are very large

due to the fractal character of these materials and because of the complexity and variety of cross-link formation [28]. Nonetheless, Shibayama *et al.* [32]–[34] have described several models for polymer gels with a strong theoretical basis. They try to separate the scattered intensity function of a polymer gel into two contributions: solution-like (dynamic) and solid-like (static) concentration fluctuations.

The solution-like concentration fluctuations are assumed to be the same as in the corresponding polymer solution. The neutron scattering intensity from a polymer solution in a semidilute regime is given by a Lorentzian function [30],

$$I(Q) = a \frac{kT(\beta_p - \beta_s)^2 \varphi^2}{K_{os}} \cdot \frac{1}{1 + \xi^2 Q^2}, \quad 9$$

where  $a$  is a constant depending on the neutron wavelength and the scattering geometry used,  $k$  is the Boltzmann constant,  $T$  is the temperature,  $\varphi$  is the polymer volume fraction,  $K_{os}$  ( $= \varphi \delta \Pi / \delta \varphi$ ) is the osmotic compressional modulus,  $\beta_p$  and  $\beta_s$  are the scattering length densities of the polymer and the solvent respectively, and  $\xi$  is the correlation length of the polymer density fluctuations in the solution. For modeling purposes, this expression can be reduced to the so-called Ornstein-Zernike equation [33],

$$I(Q) = \frac{I_L(0)}{1 + \xi^2 Q^2}, \quad 10$$

where  $I_L(0)$  is the Lorentzian intensity at  $Q = 0$ .

Formation of a polymer gel introduces cross-links, which perturb the concentration fluctuations [33]. Horkay *et al.* [30], [31] assume that the solid-like concentration fluctuations have the form  $\exp[-\Xi^s Q^s]$ , where  $\Xi$  is the mean size of the static nonuniformities and  $s$  is a positive constant. They combine this with the

solution-like expression (Equation 10) to obtain a scattering function for chemically cross-linked gels [30], which is given by [33]

$$I(Q) = I_G(0)\exp[-\Xi^s Q^s] + \frac{I_L(0)}{1+\xi^2 Q^2}, \quad 11$$

in which  $\xi$  is now the correlation length in the solution-like part of the gel and  $I_G(0)$  is the Gaussian intensity at  $Q = 0$ .

When the distribution of the cross-linked polymer regions is Gaussian, the exponent  $s$  is shown to be 2 [31]. Equation 11 then becomes the so-called Gauss-Lorentz expression for polymer gels. The equation has been capable of describing the scattering from several gels. However, as illustrated in Figure 11, the expression is not able to fit the experimental data for cellulosic resin particles. All model parameters are kept adjustable for this fit. Similarly, Shibayama *et al.* [33] observed an equally bad fit for poly(vinyl alcohol) gel; the asymptotic behavior  $I(Q) \sim Q^{-2}$  does not describe some kinds of gels. Hence, they theoretically derived a generalized Ornstein-Zernike (GOZ) expression [32],

$$I(Q) = \frac{I_L(0)}{\{1+[(D+1)/3]\xi^2 Q^2\}^{D/2}}, \quad 12$$

where  $D$  is the fractal dimension. Figure 11 illustrates how the GOZ expression fits the experimental data very well, while the OZ expression fails to do so. Note that the expressions are only fit in the intermediate- and high- $Q$  regions, as they describe only the solution-like part of the gel. The fact that there is more scattering at low- $Q$  than predicted by the model, confirms the presence of large static scatterers [31]. The calculated fractal dimension  $D$  is 2.82, which is similar to the value found by Shibayama *et al.* [33] for poly(vinyl alcohol). The exponent higher than two is attributed to the presence of hydrogen bonding in the system.

Substituting the GOZ expression in the second term of Equation 11 results in an expression that is conveniently called here the Gauss-GOZ (GGOZ) expression. As depicted in Figure 11, this expression fits the experimental data fairly well, though it fails to capture the low- $Q$  regime. As pointed out by Shibayama *et al.* [33], the Gaussian term in Equation 11 is equivalent to the well-known Guinier expression [38]. Hence, we propose to generalize this term in the same way as has been done for the Guinier expression [39]–[42]. The expression, here named the generalized Gauss-Lorentz (GGL) expression, becomes

$$I(Q) = \frac{I_G(0)}{Q^s} \exp \left[ \frac{-\Xi^s Q^s}{3-s} \right] + \frac{I_L(0)}{\{1 + [(D+1)/3] \xi^2 Q^2\}^{D/2}}. \quad 13$$

The  $s$  parameter helps model nonspherical objects: for three-dimensional globular objects (such as spheres)  $s = 0$ , for rods  $s = 1$ , and for lamellae (or platelets)  $s = 2$ . This expression has been implemented in the program IGOR Pro to fit the experimental data [22]. All model parameters are kept adjustable for this fit. The result is included in Figure 11. The model fits the experimental data well. The exponent  $s$  is evaluated as 1.83, which is between the values for rods and platelets. The fractal dimension  $D = 2.89$  is similar to the value obtained for the GOZ expression alone. The solid-like correlation length  $\Xi$  (related to clusters) and the solution-like correlation length  $\xi$  (related to pores) are 300 Å and 134 Å, respectively.

### 4.3 The Generalized Guinier-Porod Model

It should be noted that the GGL expression is in a form equivalent to the generalized Guinier-Porod (GGP) equation [43],

$$I(Q) = \frac{G}{Q^s} \exp \left[ \frac{-Q^2 R_g^2}{3-s} \right] \quad \text{for } Q \leq Q_1 \quad \text{and}$$

$$I(Q) = \frac{D}{Q^m} \quad \text{for } Q > Q_1, \quad 14$$

in which, from continuity constraints, the following relationships are valid:

$$Q_1 = \frac{1}{R_G} \sqrt{\frac{(m-s)(3-s)}{2}} \quad \text{and} \quad D = G \exp\left[\frac{-Q^2 R_G^2}{3-s}\right] Q_1^{m-s} \quad 15$$

However, the GGP equation has fewer parameters than the GGL model and can hence be seen as more elegant. In addition, Figure 11 shows that the GGP equation fits the experimental data almost equally well. The exponent  $s$  obtained from the GGP model has a value of 1.79, and the Porod exponent  $m$  equals 2.85. Consequently, the GGP model is used henceforth in the thesis to model the scattering from the pure resin particles.

The generalized Guinier-Porod fit gives one characteristic radius of gyration  $R_g$  for the whole particle structure of 43 Å, which corresponds to a generic half-size of 63 Å [43]. Interestingly, this is similar to the mean pore radius of the particle as determined earlier by Angelo *et al.* via inverse size-exclusion chromatography (ISEC) [19]. ISEC gives a mean pore size for the cylindrical pore model of 44 Å, and for the Ogston model of  $36 \pm 4$  Å. Although this does not give direct validation of the pore size, it does indicate that SANS captures structures at the right length scale, and can hence characterize the particle structure.

## Chapter 5

### PROTEIN ADSORPTION DATA ANALYSIS

This chapter uses the model from the previous chapter to characterize the difference in scattering upon protein adsorption. Section 5.1 compares the spectra with and without adsorption to distinguish two individual contributions to the total scattering after adsorption. Afterwards, Sections 5.2, 5.3, 5.4, and 5.5 discuss the background values, scaling values, and the two contributions, respectively, and compare and link them to the sample compositions.

#### 5.1 Comparison of Spectra

After removal of the background and scaling of the scattering spectra, and upon acquiring a model to describe the scattering from the pure resin particles, it is possible to compare the scattering spectra from the particles before and after protein adsorption. Figure 13 compares the reduced spectra before and after protein adsorption. Protein adsorption changes the scattering spectrum in the low- $Q$  and high- $Q$  region (regions I and II).

The scattering in the intermediate- $Q$  region is not affected by protein adsorption (region II). Arguably, this is per construction due to the definition of the scaling factors for the protein adsorption samples (Section 3.4.2). However, the full overlap of the scattering spectra in this region, even after scaling, reinforces the idea that protein adsorption does not affect this region. In addition, it is shown later in this chapter that the scaling coefficients are quantitatively correct. Finally, Yadav *et al.*

have investigated systems in which silica nanoparticles are aggregated in the presence of lysozyme [44]. The SANS data they obtain also show that the presence of proteins changes the low- and high- $Q$  region, but not the intermediate- $Q$  region.

From these observations, it is proposed that the scattering spectrum is composed of three individual, non-interacting contributions [45], *i.e.*

$$\left(\frac{d\Sigma}{d\Omega}\right)_{\text{coh}}(Q) = \left(\frac{d\Sigma}{d\Omega}\right)_p(Q) + \left(\frac{d\Sigma}{d\Omega}\right)_m(Q) + \left(\frac{d\Sigma}{d\Omega}\right)_a(Q). \quad 16$$

The three terms on the right-hand side represent the scattering from the pure resin particles, the protein monomers, and the change in structure due to the adsorption of the protein, respectively. These three contributions are discussed consecutively.

The scattering from the pure resin particles,  $(d\Sigma/d\Omega)_p(Q)$ , is assumed to be the same as the scattering without protein adsorption. This assumption has to be valid at least in the intermediate- and high- $Q$  region (regions II and III); changes in the low- $Q$  region – the one that corresponds to the particle's fractal region – can be accommodated with the third term in the equation. The scattering from the pure resin particles can be modeled with the generalized Guinier-Porod (GGP) model, as discussed in Chapter 4. Consequently, this term is assumed to be known. Subtraction of this contribution from the total scattering spectrum reveals the changes due to the addition of protein to the system. Figure 14 clearly illustrates that after subtraction of the pure resin particle scattering, two new contributions to the total scattering appear.

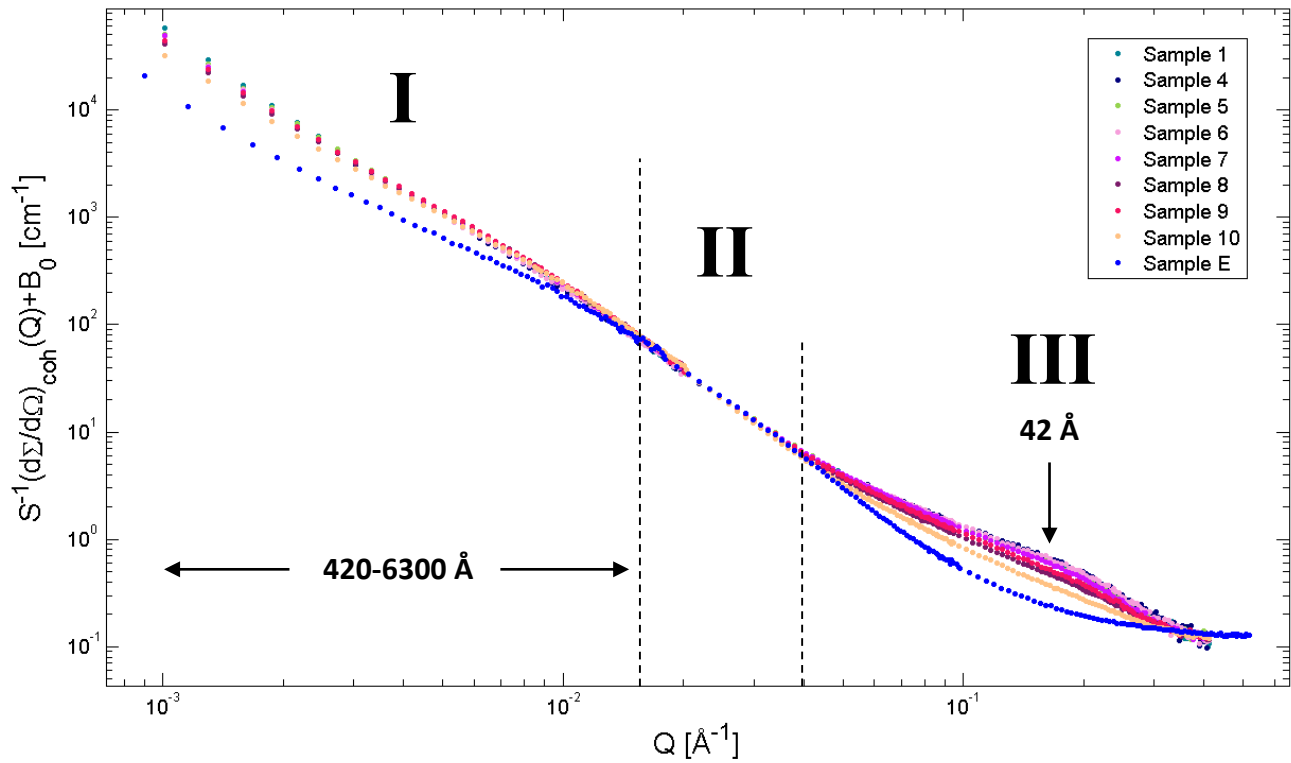


Figure 13: Comparison of the reduced spectra (with background correction and scaling) for the protein adsorption samples and the scattering from pure resin particles (sample E).

The change in scattering upon protein adsorption in the high- $Q$  region (region III) is attributed to the scattering from the protein monomers,  $(d\Sigma/d\Omega)_m(Q)$ . Protein monomers have a characteristic scattering pattern which is a form factor (shape) contribution. In addition, proteins can have a structure factor contribution due to local interactions in solution, clustering, and aggregation. The scattering spectra observed at high  $Q$ -values are consistent with those found in the literature for lysozyme monomers in solution [44], [46]–[51]. Furthermore, the scattering spectra from proteins can be calculated, as shown in Section 5.4.



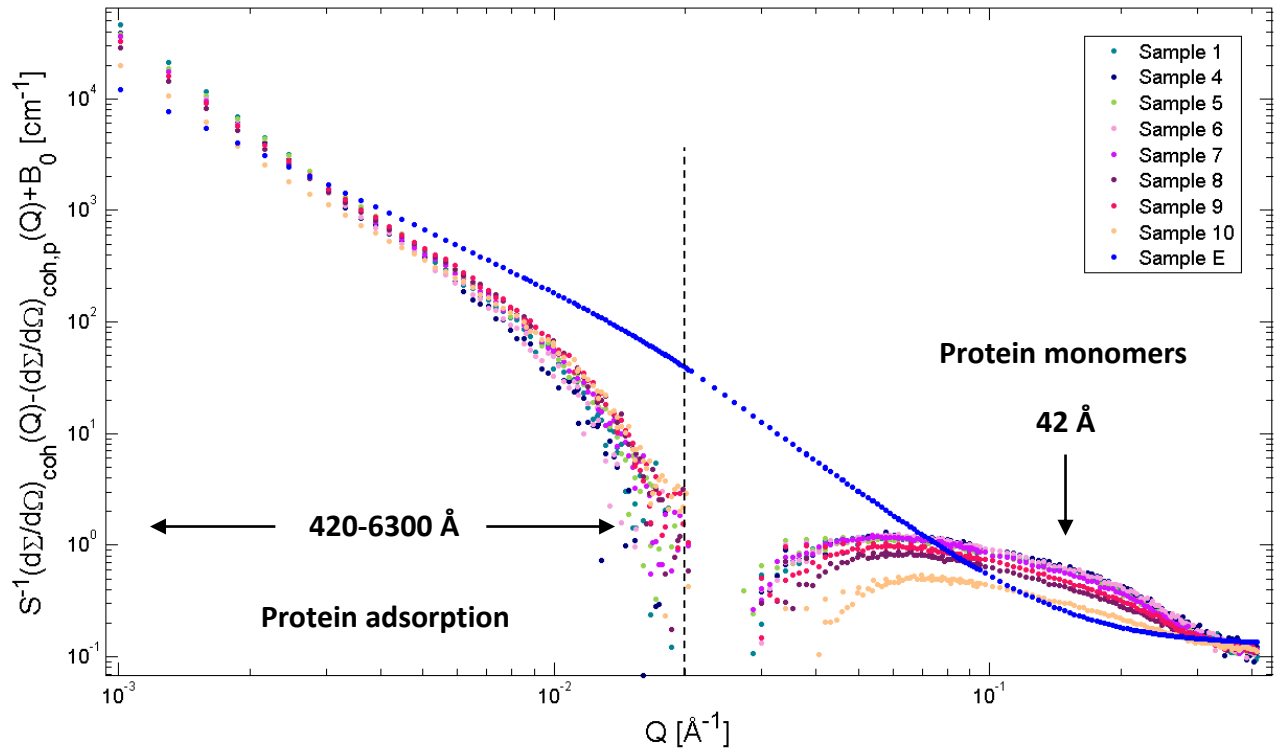


Figure 14: Scattering spectra after subtraction of the pure resin particle scattering spectrum (blue) from the total coherent scattering spectra. The result represents the change in scattering caused by the addition of protein to the system. Two contributions are identified: scattering from the protein monomers in the high- $Q$  region and a change in structure in the low- $Q$  region.

The last contribution to the total scattering spectrum is observed in the low- $Q$  region. This is the region where the fractal regime of the particle structure manifests. Consequently, it is proposed that this contribution,  $(d\Sigma/d\Omega)_m(Q)$ , is due to the adsorption of protein in the particle structure. The change is not necessarily due to an actual conformational change of the particle structure itself. Adsorption of the protein, and hence a densification of the open gel-like particle structure, might lead to a change in scattering without modifying the cellulosic backbone of the particle. This is further

discussed in Section 5.5.

## 5.2 Background

The experimentally obtained incoherent background values from the Porod plot are related to sample composition. In theory, the values can therefore be used to determine the sample composition, or conversely, the background can be predicted from the sample composition. However, the incoherent scattering originates mainly from the large incoherent scattering cross-section of the H atom,  $\sigma_{\text{inc,H}} = 82.26 \text{ b}$  ( $1 \text{ b} = 10^{-28} \text{ m}^2$ ), which is much larger than that of its isotope D,  $\sigma_{\text{inc,D}} = 2.05 \text{ b}$ , and those of other major elements for soft-matter systems, *i.e.*  $\sigma_{\text{inc,C}} = 0.001 \text{ b}$ ,  $\sigma_{\text{inc,O}} = 0.0008 \text{ b}$ , and  $\sigma_{\text{inc,N}} = 0.5 \text{ b}$  [46]. Because of this large value of  $\sigma_{\text{inc,H}}$ , multiple scattering takes place, which makes it difficult to evaluate  $(d\Sigma/d\Omega)_{\text{inc}}$  precisely [23].

Without taking multiple scattering into account, the incoherent background scattering can simply be estimated as

$$\left(\frac{d\Sigma}{d\Omega}\right)_{\text{inc}} = \frac{\Sigma_{\text{inc}}}{4\pi}, \quad 17$$

In which  $\Sigma_{\text{inc}}$  is the total macroscopic incoherent cross-section. The total macroscopic incoherent cross-section is calculated by summation of the macroscopic incoherent cross-sections of the individual compounds in the system. The incoherent cross-sections of the individual compounds are obtained from the NIST neutron activation and scattering calculator [18], which gives the incoherent cross-sections per gram of compound per milliliter. These values are shown in Table 7. Note that the incoherent scattering from lysozyme is dependent on the fraction of exchanged hydrogens. For these calculations, it is assumed that the fraction of exchanged hydrogens is equal to

the D<sub>2</sub>O: H<sub>2</sub>O fraction of the sample, *e.g.* in a 85 mole % D<sub>2</sub>O sample, 85% of the exchangeable hydrogens are exchanged for deuterium. Multiplication of the incoherent cross-section values in Table 7 by the sample compositions in Table 3 (page 18) and subsequent summation gives the total macroscopic incoherent cross-section of the sample, *i.e.*

$$\Sigma_{\text{inc}} = \sum_i c_i \Sigma_{\text{inc}}(i). \quad 18$$

In this equation, the summation is over all compounds in the sample,  $c_i$  is the concentration of the compound in the sample (g/mL), and  $\Sigma_{\text{inc}}(i)$  is the incoherent cross-section of compound  $i$  (cm<sup>-1</sup>/(g/mL)).

Table 7: Chemical formula and incoherent scattering cross-sections for the different compounds as obtained from the NIST neutron activation and scattering calculator [18].

	Cellulose	Sulfonate	D <sub>2</sub> O	H <sub>2</sub> O	NaCl	Protein (0% exchange)	Protein (100% exchange)
Chemical formula	H <sub>10</sub> C <sub>6</sub> O <sub>5</sub>	H <sub>2</sub> C <sub>1</sub> O <sub>3</sub> S <sub>1</sub>	D <sub>2</sub> O	H <sub>2</sub> O	NaCl	H <sub>962</sub> C <sub>613</sub> N <sub>193</sub> O <sub>185</sub> S <sub>10</sub>	H <sub>692</sub> D <sub>270</sub> C <sub>613</sub> N <sub>193</sub> O <sub>185</sub> S <sub>10</sub>
Incoherent scattering [cm <sup>-1</sup> /(g/mL)]	2.981	1.027	0.123	5.366	0.071	3.252	2.320

The results are shown in Table 8, along with the experimentally obtained background values. Figure 15 compares the experimentally measured values for the incoherent background with the calculated ones in the assumption of single scattering events. First, note that sample 7 and sample 10 are outliers. For sample 10, this was expected, as a big air bubble was observed in the sample cell after the scattering experiment. The reason that sample 7 is an outlier is unknown, *e.g.* it might be due to a faulty sample cell. However, that sample 7 actually is an outlier is clear from several

measured parameters, as is shown later in the thesis. Figure 15 shows that the predictions are very accurate in capturing the trend line, although they are low by a factor of  $1.99 \pm 0.10$ . Consequently, we can state that while the method is valid, the factor is probably caused by multiple scattering. This is no surprise, as we expect multiple scattering to occur.

If incoherent scattering dominates, as we expect for the high- $Q$  region, Shibayama *et al.* [23] have derived an approximation for the incoherent background scattering

$$\left(\frac{d\Sigma}{d\Omega}\right)_{\text{inc}} \cong \frac{1}{4\pi d} \frac{1-T}{T}, \quad 19$$

in which  $d$  is the sample thickness (1 mm) and  $T$  is the transmission. The transmission for the different samples is obtained during data reduction in Igor Pro [22] and is included in Table 8. Table 8 also shows the results of the approximation. Figure 16 shows the comparison between the measured and calculated values. The predictions are quantitatively correct, although the assumption of dominant incoherent scattering becomes less valid at lower background values, where less hydrogen is present.

The calculations assuming multiple scattering are quantitatively correct, but do not use the sample compositions and cannot be used for predictions, as the transmission is not known directly. The calculations assuming single scattering, on the other hand, are only qualitatively correct, but they are interesting as they directly use the sample composition. The expected background of new sample compositions can now be predicted using the single scattering method, along with the experimentally determined factor attributed to multiple scattering.

Table 8: Measured values for the incoherent background  $(d\Sigma/d\Omega)_{\text{inc}}$  for the protein adsorption experiment, along with calculated values in the cases of single and dominant multiple scattering. The ratios between the values are included. In addition, the transmission is given.

Sample	Measured [cm <sup>-1</sup> ]	Single scattering		Transmission <i>T</i> [–]	Multiple scattering	
		Calculated [cm <sup>-1</sup> ]	Ratio M/C		Calculated [cm <sup>-1</sup> ]	Ratio M/C
1	0.277	0.135	2.050	0.737	0.284	0.976
4	0.322	0.163	1.978	0.712	0.322	1.001
5	0.253	0.129	1.957	0.744	0.274	0.922
6	0.324	0.158	2.058	0.710	0.324	1.000
7	0.586	0.093	6.323	0.786	0.216	2.710
8	0.210	0.105	1.997	0.762	0.248	0.848
9	0.239	0.113	2.114	0.747	0.269	0.890
10	0.169	0.153	1.106	0.585	0.564	0.300
11	0.128	0.071	1.804	0.810	0.186	0.686

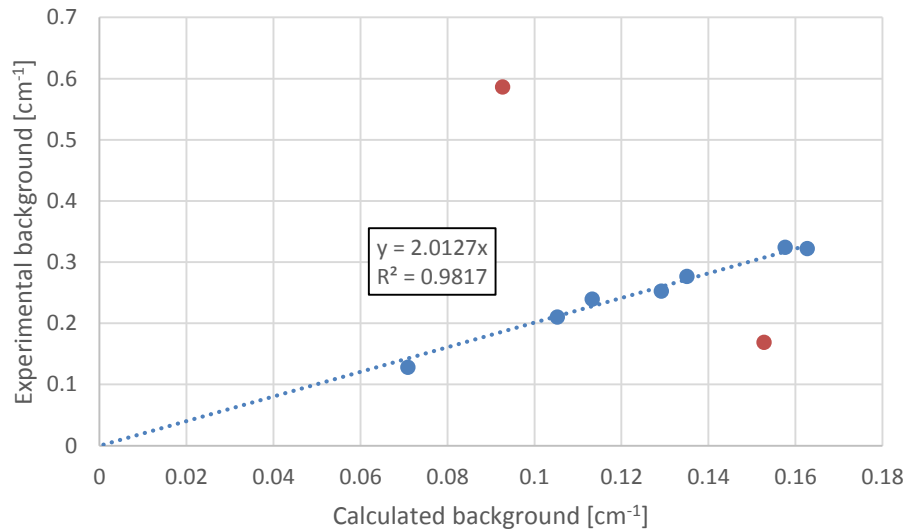


Figure 15: Comparison of the experimentally measured incoherent background values with the calculated ones for the protein adsorption experiment, assuming single scattering. The red symbols represent outlier samples (sample 7 and sample 10). The blue line is a linear least-squares fit through the origin (excluding the outliers).

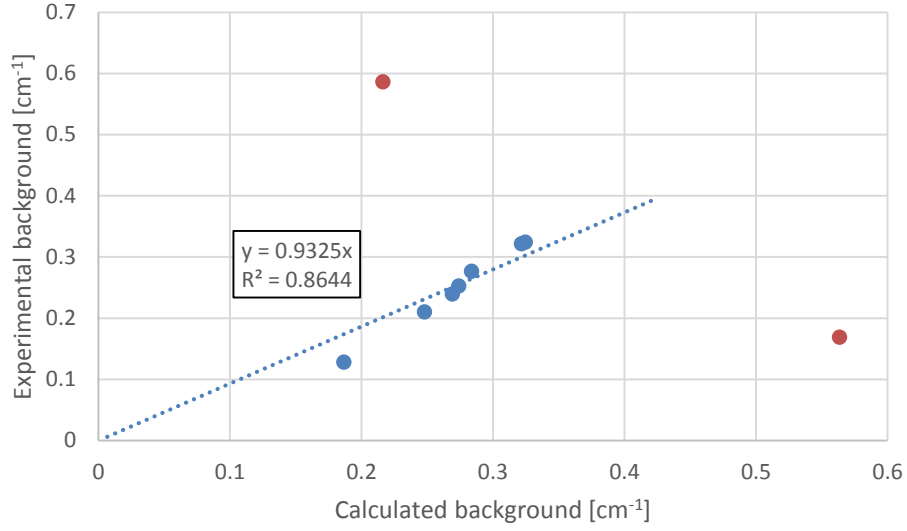


Figure 16: Comparison of the experimentally measured incoherent background values with the calculated ones for the protein adsorption experiment, assuming dominant multiple scattering. The red symbols represent outlier samples (sample 7 and sample 10). The blue line is a linear least-squares fit through the origin (excluding the outliers).

### 5.3 Scaling

From Equation 4 (page 6), we know that the scattering intensity, and hence the scaling of the scattering spectra, is related to the contrast factor, *i.e.*

$$\left(\frac{d\Sigma}{d\Omega}\right)_{\text{coh}}(Q) \propto (\beta_p - \beta_s)^2 = \Delta\beta^2.$$

In the case of the contrast matching experiment, this is the only difference between the samples, and the scaling factor  $S = \Delta\beta^2$ . For the protein adsorption experiment, the composition of the samples changes, and this might also scale the intensity as *e.g.* the total number of scatterers changes. Still, Equation 4 remains valid and we can expect that the scaling factor  $S \propto \Delta\beta^2$ .

The contrast factors can be calculated by combining Equation 4 and Equation 8 (page 25), where the D<sub>2</sub>O: H<sub>2</sub>O fraction of the solutions is obtained from Table 3 (page

18) after conversion to molar concentrations. These fractions are given in Table 9. The scattering length densities for D<sub>2</sub>O, H<sub>2</sub>O, and the cellulosic resin particles are  $6.33 \times 10^{-6} \text{ \AA}^{-2}$ ,  $-5.60 \times 10^{-7} \text{ \AA}^{-2}$ , and  $2.06 \times 10^{-6} \text{ \AA}^{-2}$ , respectively. The calculated contrast factors for the samples are included in Table 9, along with the measured scaling factors.

Figure 17 compares the measured scaling factors to the calculated contrast factors. Indeed, there is a relation between them that seems to be linear, although there is significant scatter for different samples.

#### 5.4 Protein Monomers

After subtraction of the pure resin particle contribution, the monomer contribution from lysozyme appears clearly in the high- $Q$  region (Figure 14, page 41). The ‘bump’, starting at high  $Q$  around  $0.3 \text{ \AA}^{-1}$  and increasing with decreasing  $Q$  up to a plateau value around  $0.07 \text{ \AA}^{-1}$ , is the characteristic lysozyme monomer form factor as reported before [44], [47]–[49]. The subsequent drop of scattering intensity as  $Q$  decreases towards  $0.03 \text{ \AA}^{-1}$  is believed to be an artifact due to the subtraction of the pure resin particle contribution and not a real feature of the scattering curve. It should be noted that such a peak around  $Q \approx 0.07 \text{ \AA}^{-1}$  has been reported for concentrated lysozyme solutions [47], [48], [50]–[52]. In these cases, the peak originates from the structure factor of the intermediate range order (IRO) structure, previously inappropriately termed the ‘cluster peak’ [50], [51]. However, the assumption that the peaks in our experiment are artificial can be supported by the dissimilar shape of the peaks compared to those in the literature, and the fact that the interaction peak has been shown to disappear at the higher TISs used here [47], [48].

Table 9: Values of the experimental scaling factors  $S$ , along with the calculated values of the contrast factor  $\Delta\beta^2$ . In addition, the D<sub>2</sub>O: H<sub>2</sub>O fractions, necessary for the calculation, are included.

Sample	Experimental scaling factor $S$ [-]	D <sub>2</sub> O: H <sub>2</sub> O fraction [mole%]	Contrast factor $\Delta\beta^2$ [ $10^{-12} \times \text{\AA}^{-4}$ ]
1	0.260	0.863	11.09
4	0.213	0.779	7.55
5	0.325	0.879	11.82
6	0.232	0.794	8.14
7	0.645	0.967	16.36
8	0.490	0.940	14.87
9	0.447	0.921	13.87
10	0.609	0.836	9.88

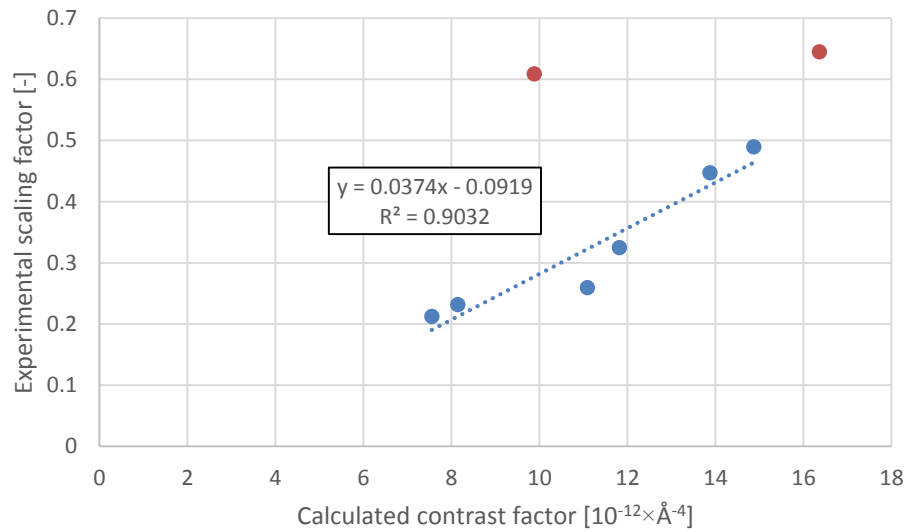


Figure 17: Comparison of the experimentally measured scaling factor  $S$  values with the calculated contrast factors  $\Delta\beta^2$  for the protein adsorption experiment. The red symbols represent outlier samples (sample 7 and sample 10). The blue line is a linear least squares fit (excluding the outliers).



Hence, we propose that the protein monomer contribution is dominated by the lysozyme form factor. This is illustrated more clearly in Figure 18, which tries to negate the effect of the pure resin particle contribution subtraction. Instead of subtracting the full pure resin particle contribution, the figure shows the result if this contribution is first reduced by a factor 0.9 before subtraction. This factor is chosen so as to make the protein monomer contribution reach a plateau value at lower  $Q$ -values, instead of dipping down. Although this seems rather arbitrary, the plateau value is present in experimental lysozyme scattering curves. The absence of peaks in this figure supports the idea that the peaks in Figure 14 are artifacts, and that the structure factor contribution is negligible.

The lysozyme form factor is obtained with the program CRYSON [53]. CRYSON calculates the form factor of a protein from its atomic structure as available from the Protein Data Bank (PDB), and can take several effects such as the solvation shell (not applied here) and the solvent composition (100 mole %  $D_2O$ ) into account. The CRYSON output is the absolute scattering form factor of a single protein monomer in units of barn ( $1 \text{ b} = 10^{-28} \text{ m}^2$ ). Multiplication of this spectrum by the total number of protein monomers per volume in the system yields the total protein form factor contribution. Thus, we can predict the protein monomer contribution from the protein concentration in the system, or conversely, we can determine the protein concentration from the protein monomer contribution to the scattering intensity. Figure 18 shows the protein monomer form factor spectrum as obtained by CRYSON for a lysozyme concentration of  $4.5 \times 10^{-6} \text{ mole/mL}$  or  $64.4 \text{ mg/mL}$  (MW lysozyme 14.3 kD). The predicted curve is reasonable, although it does not fully capture the high- $Q$  behavior.

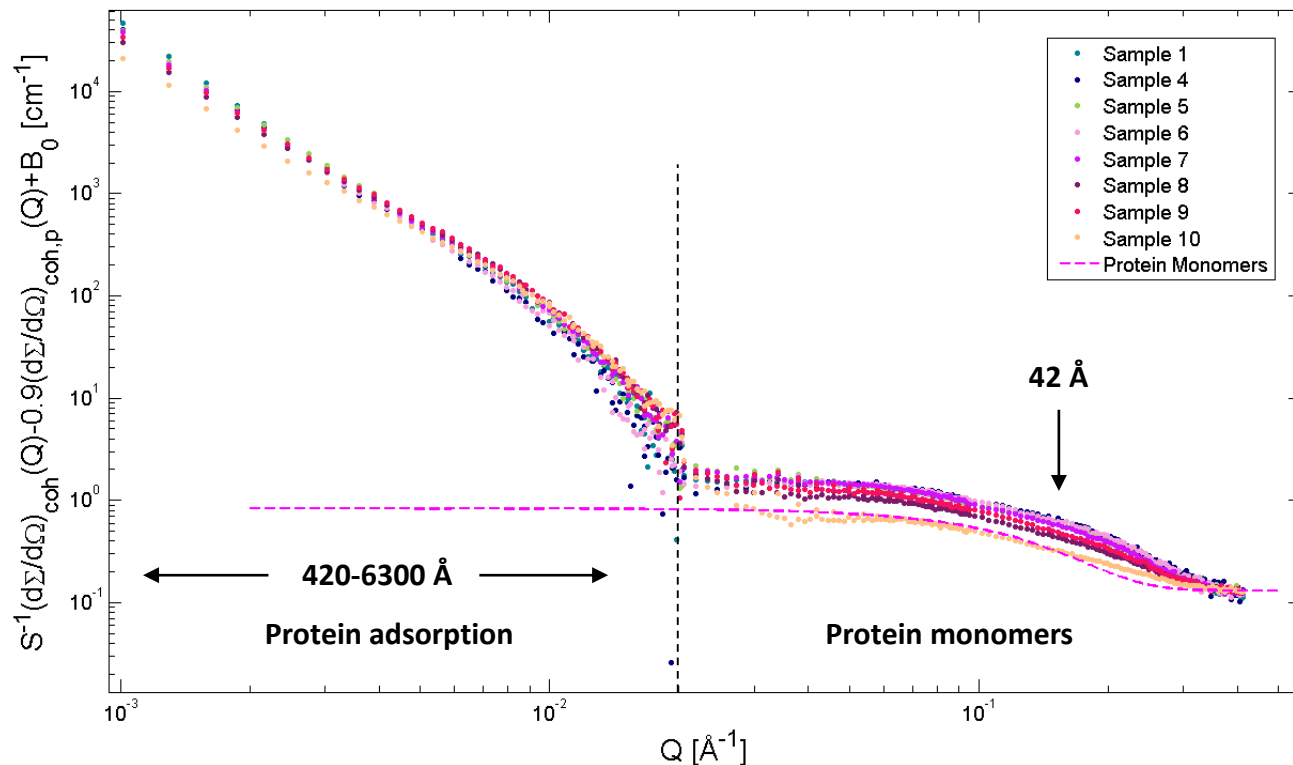


Figure 18: Scattering spectra after subtraction of the pure resin particle scattering spectrum from the total coherent scattering spectra. The pure resin particle spectrum is first reduced by a factor 0.9 to negate the artifact due to the subtraction and scaling assumptions. The protein form factor as calculated by CRYSON for a  $4.5 \times 10^{-6}$  mole/mL solution is shown in magenta.

Figure 19 shows the least-squares fitting of the form factor spectrum as calculated by CRYSON to the experimentally determined protein monomer contributions. Indeed, the fit at the higher  $Q$ -values shows significant deviation, though this is not critical as the protein concentration is determined by the plateau

value at a lower  $Q$ . The deviation can be caused by several factors, including the amount of exchanged hydrogens, the temperature [50], the solvation shell, and the lysozyme structure in the PDB-file. In addition, if the pure particle model does not capture the actual data perfectly, the pure particle contribution does not get subtracted correctly and leaves a resultant error in the protein monomer contribution, which is especially sensitive at these high  $Q$ -values or low intensities. Note that the CRYSON curve is fitted to the fully subtracted spectra (without the 0.9 scaling factor), as is appropriate. The dip at lower  $Q$ -values is ignored by fitting for  $Q \geq 0.05 \text{ \AA}^{-1}$ . From the scaling factor, we can immediately obtain the protein concentration. These predicted protein concentrations are shown in Table 10, along with the actual protein concentrations in the samples. These actual protein concentrations include both the adsorbed protein and the protein in solution. Figure 20 presents these results graphically.

The results are quantitatively correct, with a ratio between predicted and actual values of  $1.03 \pm 0.04$ . This has several important consequences. Firstly, this means of course that we can calculate the protein concentration in the system from the scattering spectrum. Further, this indicates that the scaling method used to scale the scattering spectra was correct. Note that it is important that we scaled the spectra to the 100 mole %  $D_2O$  curve (sample E), while the form factor calculated with CRYSON is also for a 100 mole %  $D_2O$  solution. The validation of the scaling method proves that the scattering in the intermediate- $Q$  region is indeed independent of the protein adsorption. Finally, it is clear that the adsorbed protein still contributes to the monomer scattering spectrum, along with the protein in solution. This indicates that the protein still retains its monomer character even after adsorption.

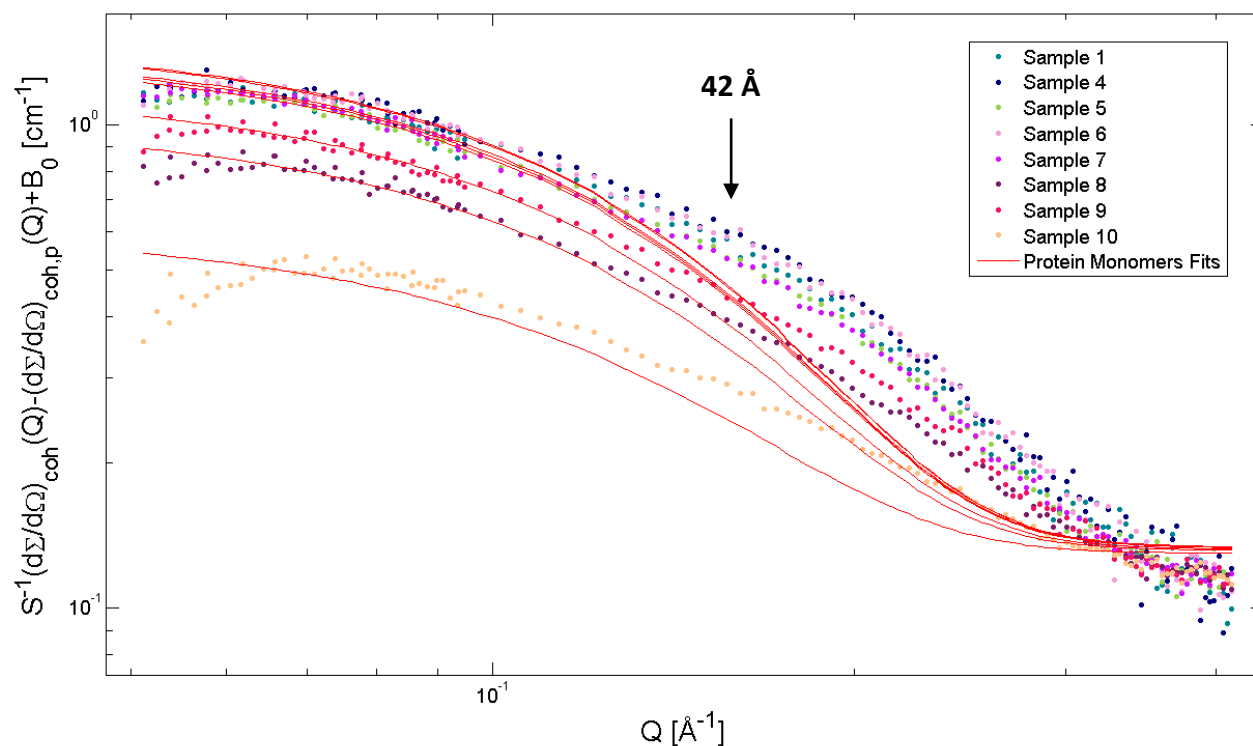


Figure 19: Fitting of the protein form factor spectra as calculated by CRYSON (red) to the experimentally obtained protein monomer contributions for the protein adsorption experiment.

Table 10: Predicted and actual protein concentrations in the samples. The ratio is also included.

Sample	Predicted concentration [mg/mL]	Actual concentration [mg/mL]	Ratio P/A
1	119.56	116.87	1.02
4	125.81	117.49	1.07
5	115.98	110.49	1.05
6	124.78	116.67	1.07
7	118.00	61.44	1.92
8	81.13	83.80	0.97
9	96.73	95.31	1.01
10	43.77	178.27	0.25

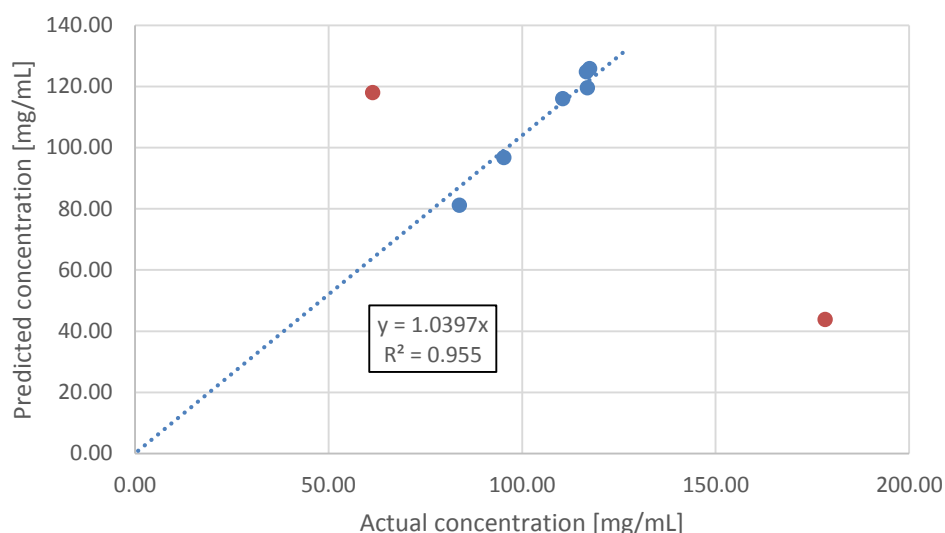


Figure 20: Comparison of the predicted protein concentrations (via CRYSON and least-squares fitting) with the actual sample concentrations for the protein adsorption experiment. The red symbols represent outlier samples (sample 7 and sample 10). The blue line is a linear least-squares fit through the origin (excluding the outliers).

## 5.5 Protein Adsorption

The last contribution to the total incoherent scattering spectrum is the change in particle structure due to protein adsorption. This change can be both an actual change in the cellulosic backbone of the particle, and a filling of the particle due to protein positioning in the particle voids. Figure 13 (page 40) shows that the particle adsorption changes only the dimension of the fractal region of the particle structure. There is no formation of peaks or other local interactional effects in the scattering spectrum visible. This indicates that the protein adsorbs rather uniformly throughout the particle, without effects such as clustering or aggregation of the protein in specific domains of the particle. In addition, we know that the protein and the cellulosic backbone of the particle have a very similar scattering length density. Thus, the

adsorption of the protein inside the particle structure can be seen as a densification of the cellulosic particle gel-like structure (recall the discussion in Chapter 4). The increase in fractal dimension corresponds to this hypothesis.

Figure 14 (page 41) shows that the protein adsorption contribution is indeed another fractal term. Figure 21 illustrates the linear least-squares fit of this term to determine the fractal dimension. It is clear that these slopes are very similar, almost indiscernible to the naked eye. Table 11 summarizes the results, along with the protein adsorption  $q$  in the samples and the TIS. Indeed, we expect that the densification in the system, and hence the slope or fractal dimension, is proportional to the protein adsorption. Figure 22 illustrates that there is a trend, although it is weak. More controlled experiments, with a wider range of adsorbed amount of protein  $q$ -values, are necessary to get a more definitive relation between these values.

Another relation might be found between the TIS and the fractal dimension, as a change in the TIS might lead to a partial collapse of the particle and adsorbed protein structure. Again, while Figure 23 indicates that this might be the case, experimental evidence is inadequate to fully support this theory.

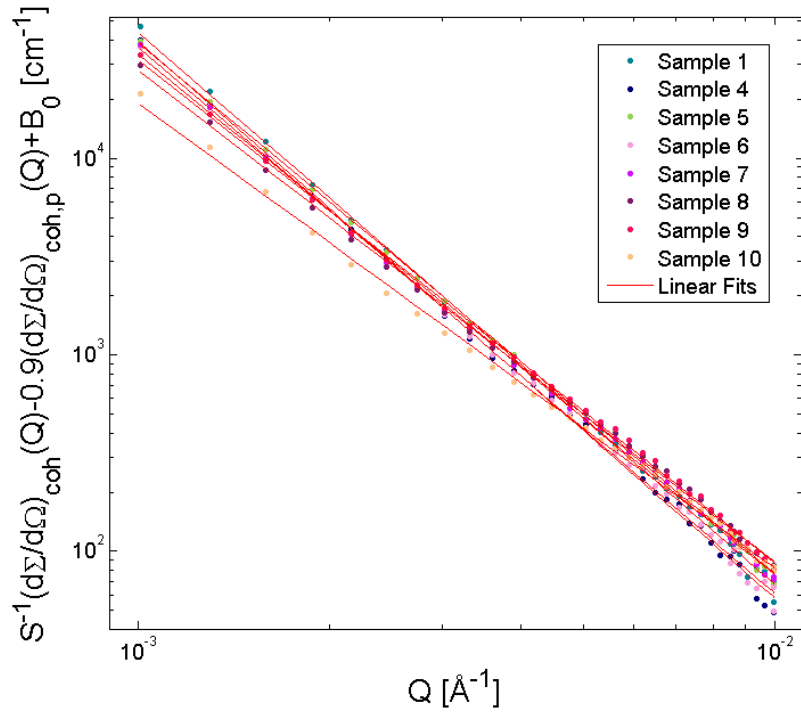


Figure 21: Linear fitting (red) of the fractal dimension of the protein adsorption contribution to the total coherent scattering in the protein adsorption experiment.

Table 11: Experimentally obtained values for the fractal dimension of the protein adsorption contribution, along with the adsorption  $q$  and the TIS.

Sample	Fractal dimension	Adsorption $q$ [mg/mL hpv]	TIS [mM]
1	2.81	109.7	35.2
4	2.83	102.7	33.5
5	2.70	105.2	88.8
6	2.78	104.6	84.5
7	2.65	60.9	186.5
8	2.51	81.6	183.7
9	2.55	91.8	181.8
10	2.37	170.8	173.0

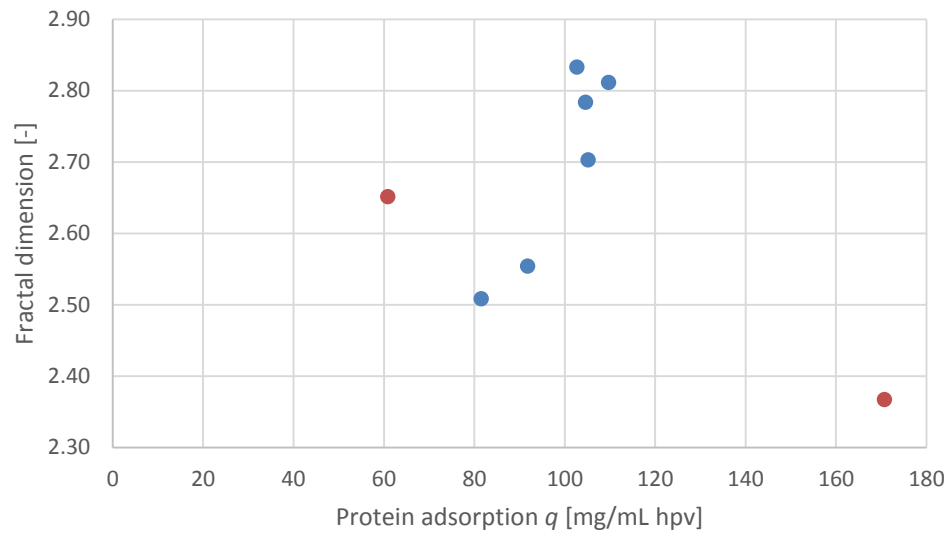


Figure 22: Comparison of the experimentally measured fractal dimension of the protein adsorption contribution with the protein adsorption  $q$ . The red symbols represent outlier samples (sample 7 and sample 10).

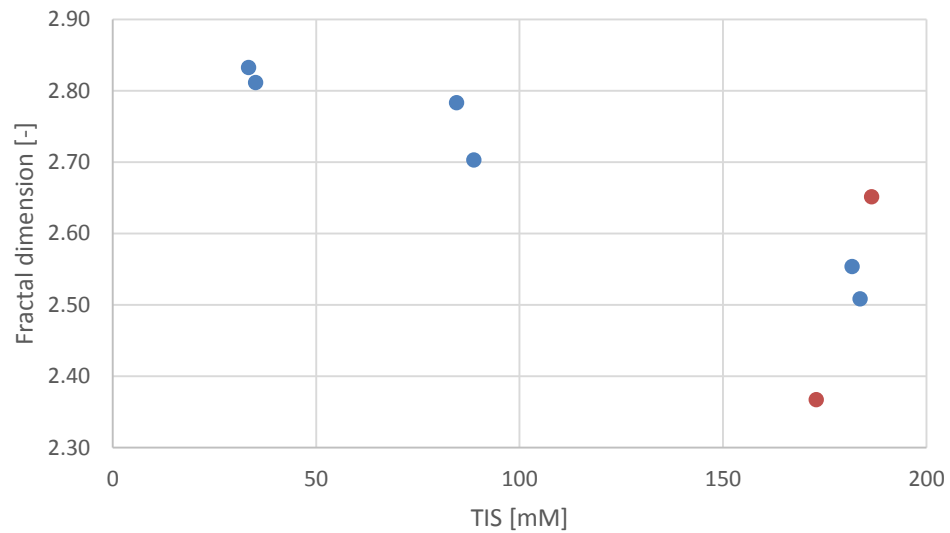


Figure 23: Comparison of the experimentally measured fractal dimension of the protein adsorption contribution with the TIS. The red symbols represent outlier samples (sample 7 and sample 10).



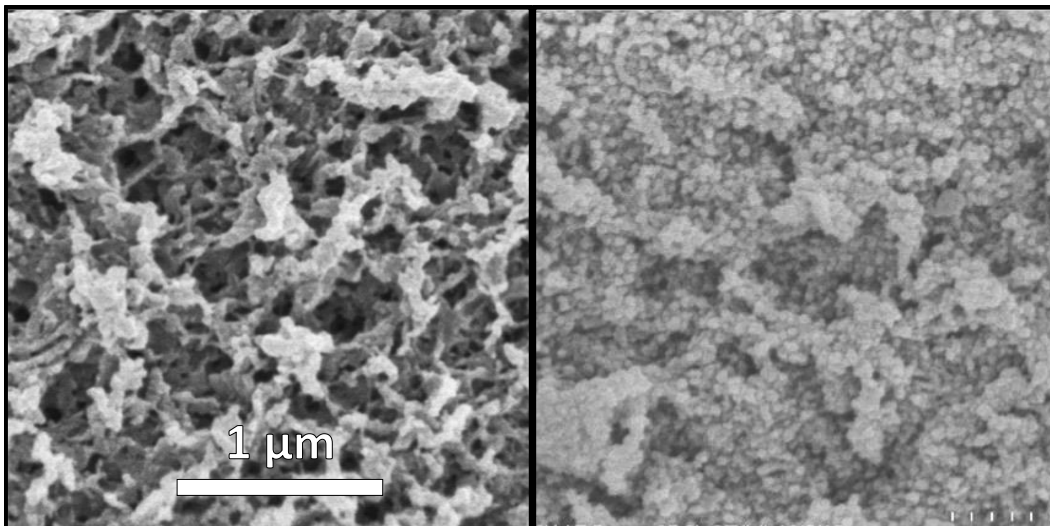


Figure 24: SEM images of Q HyperCel chemically fixed with  $\text{OsO}_4$ , without (left) and with (right) adsorption of approximately 50% of the maximum capacity of  $\beta$ -lactoglobulin [19], [20].

Evidence that lysozyme adsorption leads to a uniform densification of the particle gel-like structure is illustrated by scanning electron microscopy (SEM) images. Figure 24 shows SEM images of Q HyperCel chemically fixed with  $\text{OsO}_4$ , with and without adsorption of approximately 50% of the maximum capacity of  $\beta$ -lactoglobulin [19], [20]. Q and S HyperCel are assumed to have almost identical architectures, as the only fundamental difference is in the ion-exchange ligands. The fibrous network shown is characteristic of natural carbohydrate polymer adsorbents, and appears to contain “pores” on the order of 100 – 500 Å in characteristic dimension. After adsorption, the protein fills these pores and effectively further densifies the gel-like structure of the resin particles.

## Chapter 6

### CONCLUSIONS AND FUTURE WORK

The thesis shows that small-angle neutron scattering (SANS) is a feasible and interesting technique to characterize protein adsorption on polymer-derivatized chromatographic particles. The scattering spectra with and without protein adsorption show clear differences. However, basic contrast matching by varying the solution's D<sub>2</sub>O: H<sub>2</sub>O ratio is not viable to study the protein structure after adsorption, as the scattering length densities (SLDs) of the cellulosic particles and protein are similar. The scattering length density of the resin particles is shown to be  $2.06 \times 10^{-6} \text{ \AA}^{-2}$ , which corresponds to a contrast match point (CMP) of 38 mole % D<sub>2</sub>O. In comparison, the SLD of lysozyme is calculated to be  $1.94 \times 10^{-6} \text{ \AA}^{-2}$  for a 0 mole % D<sub>2</sub>O solution and  $2.56 \times 10^{-6} \text{ \AA}^{-2}$  for a 38 mole % D<sub>2</sub>O solution. An interesting research topic for future work would be to deuterate the protein or cellulosic particle to allow the use of contrast matching.

Instead of using contrast matching, the thesis presents a framework to allow the quantitative study of protein adsorption in these systems, by direct comparison of the scattering spectra with and without protein adsorption. To do this, the thesis proposes generally applicable methods to fully reduce the data to allow quantitative discussion of the results. These methods include accurate incoherent background removal via a Porod plot and contrast scaling based on physical considerations.

Furthermore, the thesis presents a theoretical model for the scattering from cellulosic gel-like particles to support the data interpretation. It illustrates how this

model can be obtained from experimental data, based on thermodynamic considerations and derivations from the literature. The resulting model fits the experimental data well, and can be compared to the generalized Guinier-Porod model to limit the number of parameters. Henceforth, this model can be used to fit and predict scattering data from cellulosic resin particles, although further investigation into the model parameters is required. A better understanding of how the model parameters link to particle properties will greatly encourage future use of the model.

With the help of the model for the pure resin particle scattering spectrum, we have shown that protein adsorption leads to two major individual contributions to the scattering spectrum. The first contribution is due to the form factor of protein monomers that is evident at high momentum transfer vector  $Q$ -values. The second contribution is due to the actual adsorption of the protein inside the particle structure, and is characterized by a change of the particle's fractal dimension at low  $Q$ -values. In the intermediate- $Q$  region, the protein adsorption has no effect on the scattering spectrum. Hence, it is shown that the total scattering spectrum upon protein adsorption is composed of three contributions: (1) the pure particle without adsorbed protein as captured by the theoretically derived model, (2) the form factor of protein monomers, and (3) the change in the fractal dimension of the pure particles.

The strength of these contributions, together with the values for the incoherent background and the contrast scaling, have been related to the sample compositions. The sample incoherent background can be predicted from the sample composition, and the total concentration of protein in the sample can be accurately acquired from the SANS spectrum. In general, the results support the idea that the protein adsorbs uniformly in the particle structure, and that this leads to a densification of the

cellulosic gel-like particle structure. However, more experiments at a broader range of better controlled adsorption values  $q$  and total ionic strengths (TISs) can provide better understanding of the evolution of the particle structure upon adsorption. In addition, it is advisable to tightly control the amount of protonated water  $H_2O$  in the system, as it has been shown that this significantly affects both the incoherent background and the scaling of the scattering spectra. Furthermore, other neutron scattering methods might provide additional information about the protein adsorption process, *e.g.* neutron spin echo (NSE) can be used to study the protein diffusion coefficients in the system [52]. In conclusion, the thesis provides the framework upon which such further studies of protein adsorption in chromatographic media can be built.

## REFERENCES

- [1] M. Hedhammar, A. E. Karlström, and S. Hober, “Chromatographic methods for protein purification,” Stockholm, Sweden, 2006.
- [2] D.-M. Wang, G. Hao, Q.-H. Shi, and Y. Sun, “Fabrication and characterization of superporous cellulose bead for high-speed protein chromatography,” *J. Chromatogr. A*, vol. 1146, no. 1, pp. 32–40, 2007.
- [3] K.-F. Du, M. Yan, Q.-Y. Wang, and H. Song, “Preparation and characterization of novel macroporous cellulose beads regenerated from ionic liquid for fast chromatography,” *J. Chromatogr. A*, vol. 1217, no. 8, pp. 1298–1304, 2010.
- [4] S. J. Traylor, “Novel Approaches to Understand and Predict Multicomponent Protein Sorption and Kinetics in Chromatographic Materials,” University of Delaware, 2013.
- [5] E. Müller, “Properties and Characterization of High Capacity Resins for Biochromatography,” *Chem. Eng. Technol.*, vol. 28, no. 11, pp. 1295–1305, Nov. 2005.
- [6] W. de Oliveira and W. G. Glasser, “Hydrogels from polysaccharides. I. Cellulose beads for chromatographic support,” *J. Appl. Polym. Sci.*, vol. 60, no. 1, pp. 63–73, Apr. 1996.
- [7] G. Walsh, “Biopharmaceutical benchmarks 2010,” *Nat. Biotechnol.*, vol. 28, no. 9, pp. 917–24, Sep. 2010.
- [8] A. M. Lenhoff, “Protein adsorption and transport in polymer-functionalized ion-exchangers,” *J. Chromatogr. A*, vol. 1218, no. 49, pp. 8748–8759, Dec. 2011.
- [9] T. M. Przybycien, N. S. Pujar, and L. M. Steele, “Alternative bioseparation operations: life beyond packed-bed chromatography,” *Curr. Opin. Biotechnol.*, vol. 15, no. 5, pp. 469–78, Oct. 2004.

- [10] J. Thömmes and M. Etzel, “Alternatives to chromatographic separations,” *Biotechnol. Prog.*, vol. 23, no. 1, pp. 42–5, 2007.
- [11] R. Hahn, “Methods for characterization of biochromatography media,” *J. Sep. Sci.*, vol. 35, no. 22, pp. 3001–3032, Nov. 2012.
- [12] E. Karlsson, L. Rydén, and J. Brewer, *Protein Purification: Principles, High-Resolution Methods, and Applications*. New York: Wiley-VCH, 1998.
- [13] I. Grillo, “Small-Angle Neutron Scattering and Applications in Soft Condensed Matter,” in *Soft-Matter Characterization*, LXXII., R. Borsali and R. Pecora, Eds. Berlin: Springer, 2008, pp. 705–764.
- [14] B. Hammouda, “Probing Nanoscale Structures - The SANS Toolbox,” Gaithersburg, MD, 2010.
- [15] D. S. Sivia, *Elementary Scattering Theory*, First edit. New York: Oxford University Press, 2011, p. 201.
- [16] S. Krueger, A. Andrews, and R. Nossal, “Small angle neutron scattering studies of structural characteristics of agarose gels,” *Biophys. Chem.*, vol. 53, pp. 85–94, 1994.
- [17] W. S. Dubner, J. M. Schultz, and G. D. Wignall, “Estimation of incoherent backgrounds in SANS studies of polymers,” *J. Appl. Crystallogr.*, vol. 23, no. 6, pp. 469–475, Dec. 1990.
- [18] P. Kienzle, “Neutron activation and scattering calculator,” *NIST Center for Neutron Research*, 2014. [Online]. Available: <http://www.ncnr.nist.gov/resources/activation/>.
- [19] J. M. Angelo, A. Cvetkovic, R. Gantier, and A. M. Lenhoff, “Characterization of cross-linked cellulosic ion-exchange adsorbents: 1. Structural properties,” *J. Chromatogr. A*, vol. 1319, pp. 46–56, Dec. 2013.
- [20] J. M. Angelo, A. Cvetkovic, R. Gantier, and A. M. Lenhoff, “Characterization of cross-linked cellulosic ion-exchange adsorbents: 2. Protein Sorption and Transport,” *In preparation*.
- [21] Y.-X. Bai and Y.-F. Li, “Preparation and characterization of crosslinked porous cellulose beads,” *Carbohydr. Polym.*, vol. 64, no. 3, pp. 402–407, 2006.

- [22] S. R. Kline, "Reduction and analysis of SANS and USANS data using IGOR Pro," *J. Appl. Crystallogr.*, vol. 39, no. 6, pp. 895–900, Nov. 2006.
- [23] M. Shibayama, T. Matsunaga, and M. Nagao, "Evaluation of incoherent scattering intensity by transmission and sample thickness," *J. Appl. Crystallogr.*, vol. 42, no. 4, pp. 621–628, Jun. 2009.
- [24] A. N. Fernandes, L. H. Thomas, C. M. Altaner, P. Callow, V. T. Forsyth, D. C. Apperley, C. J. Kennedy, and M. C. Jarvis, "Nanostructure of cellulose microfibrils in spruce wood," *Proc. Natl. Acad. Sci. U. S. A.*, vol. 108, no. 47, pp. E1195–E1203, Nov. 2011.
- [25] J. Crawshaw, M. Vickers, and N. Briggs, "The hydration of TENCEL® cellulose fibres studied using contrast variation in small angle neutron scattering," *Polymer (Guildf)*, vol. 41, no. 5, pp. 1873–1881, 2000.
- [26] G. Evmenenko, V. Alexeev, and H. Reynaers, "Structural study of polysaccharide films by small-angle neutron scattering," *Polymer (Guildf)*, vol. 41, pp. 1947–1951, 2000.
- [27] D. Myatt and L. Clifton, "Protein Neutron Scattering Length Density Calculator," *ISIS*, 2014. [Online]. Available: <http://psldc.isis.rl.ac.uk/Psldc/>.
- [28] N. Fatin-Rouge, K. J. Wilkinson, and J. Buffle, "Combining small angle neutron scattering (SANS) and fluorescence correlation spectroscopy (FCS) measurements to relate diffusion in agarose gels to structure," *J. Phys. Chem. B*, vol. 110, no. 41, pp. 20133–20142, Oct. 2006.
- [29] A. Hecht, R. Duplessix, and E. Geissler, "Structural inhomogeneities in the range 2.5-2500 Å in polyacrylamide gels," *Macromolecules*, vol. 18, no. 11, pp. 2167–2173, 1985.
- [30] F. Horkay, A. Hecht, and S. Mallam, "Macroscopic and microscopic thermodynamic observations in swollen poly (vinyl acetate) networks," *Macromolecules*, vol. 24, no. 10, pp. 2896–2902, 1991.
- [31] S. Mallam, F. Horkay, and A. Hecht, "Microscopic and macroscopic thermodynamic observations in swollen poly (dimethylsiloxane) networks," *Macromolecules*, pp. 543–548, 1991.
- [32] M. Shibayama, H. Kurokawa, S. Nomura, M. Muthukumar, R. S. Stein, and S. Roy, "Small-angle neutron scattering from poly(vinyl alcohol)-borate gels," *Polymer (Guildf)*, vol. 33, no. 14, pp. 2883–2890, Jan. 1992.

- [33] M. Shibayama, T. Tanaka, and C. C. Han, "Small angle neutron scattering study on poly(N-isopropyl acrylamide) gels near their volume-phase transition temperature," *J. Chem. Phys.*, vol. 97, no. 9, p. 6829, 1992.
- [34] M. Shibayama, "Small-angle neutron scattering on polymer gels: phase behavior, inhomogeneities and deformation mechanisms," *Polym. J.*, vol. 43, no. 1, pp. 18–34, Nov. 2010.
- [35] P. Schmidt, "Small-angle scattering studies of disordered, porous and fractal systems," *J. Appl. Crystallogr.*, vol. 24, no. 5, pp. 414–435, 1991.
- [36] J. Teixeira, "Small-angle scattering by fractal systems," *J. Appl. Crystallogr.*, vol. 21, no. 6, pp. 781–785, Dec. 1988.
- [37] E. Mendes, P. Lutz, J. Bastide, and F. Boue, "Soft Order in High-Functionality Star Polymer Solutions and Gels: A Small-Angle Neutron Scattering Study," *Macromolecules*, vol. 28, no. 1, pp. 174–179, Jan. 1995.
- [38] A. Guinier and G. Fournet, *Small-Angle Scattering of X-rays*, First Edit. New York: John Wiley and Sons, 1955, p. 268.
- [39] O. Glatter and O. Kratky, *Small-Angle X-ray Scattering*, ch. 4. London: Academic Press, 1982, pp. 155–156.
- [40] R. P. Hjelm, P. Thiagarajan, and H. Alkan-Onyuksel, "Organization of phosphatidylcholine and bile salt in rodlike mixed micelles," *J. Phys. Chem.*, vol. 96, no. 21, pp. 8653–8661, Oct. 1992.
- [41] O. Kratky, "X-ray small angle scattering with substances of biological interest in diluted solutions," *Prog. Biophys. Mol. Biol.*, vol. 13, p. 1963, 1963.
- [42] V. Luzzati, "Interprétation des mesures absolues de diffusion centrale des rayons X en collimation ponctuelle ou linéaire: Solutions de particules globulaires et de bâtonnets," *Acta Crystallogr.*, vol. 13, no. 11, pp. 939–945, Nov. 1960.
- [43] B. Hammouda, "A new Guinier–Porod model," *J. Appl. Crystallogr.*, vol. 43, no. 4, pp. 716–719, May 2010.
- [44] I. Yadav, S. Kumar, V. K. Aswal, and J. Kohlbrecher, "Small-angle neutron scattering study of differences in phase behavior of silica nanoparticles in the presence of lysozyme and bovine serum albumin proteins," *Phys. Rev. E*, vol. 89, no. 3, p. 032304, Mar. 2014.



- [45] S. Kumar, V. K. Aswal, and J. Kohlbrecher, "Size-dependent interaction of silica nanoparticles with different surfactants in aqueous solution," *Langmuir*, vol. 28, no. 25, pp. 9288–9297, Jun. 2012.
- [46] V. F. Sears, "Neutron scattering lengths and cross sections," *Neutron News*, vol. 3, no. 3, pp. 26–37, 1992.
- [47] A. Shukla, E. Mylonas, E. Di Cola, S. Finet, P. Timmins, T. Narayanan, and D. I. Svergun, "Absence of equilibrium cluster phase in concentrated lysozyme solutions," *Proc. Natl. Acad. Sci. U. S. A.*, vol. 105, no. 13, pp. 5075–5080, Apr. 2008.
- [48] O. D. Velev, E. W. Kaler, and A. M. Lenhoff, "Protein interactions in solution characterized by light and neutron scattering: comparison of lysozyme and chymotrypsinogen," *Biophys. J.*, vol. 75, no. 6, pp. 2682–2697, Dec. 1998.
- [49] R. Giordano, A. Grasso, and J. Teixeira, "Small-angle neutron scattering in lysozyme solutions," *Phys. Rev. A*, vol. 43, no. 12, pp. 6894–6899, 1991.
- [50] P. Falus, L. Porcar, E. Fratini, W.-R. Chen, A. Faraone, K. Hong, P. Baglioni, and Y. Liu, "Distinguishing the monomer to cluster phase transition in concentrated lysozyme solutions by studying the temperature dependence of the short-time dynamics," *J. Phys. Condens. Matter*, vol. 24, no. 6, p. 064114, Feb. 2012.
- [51] Y. Liu, L. Porcar, J. Chen, W.-R. Chen, P. Falus, A. Faraone, E. Fratini, K. Hong, and P. Baglioni, "Lysozyme protein solution with an intermediate range order structure," *J. Phys. Chem. B*, vol. 115, no. 22, pp. 7238–7247, Jun. 2011.
- [52] L. Porcar, P. Falus, W.-R. Chen, A. Faraone, E. Fratini, K. Hong, P. Baglioni, and Y. Liu, "Formation of the Dynamic Clusters in Concentrated Lysozyme Protein Solutions," *J. Phys. Chem. Lett.*, vol. 1, no. 1, pp. 126–129, Jan. 2010.
- [53] D. Svergun, C. Barberato, and M. Koch, "CRY SOL - a Program to Evaluate X-ray Solution Scattering of Biological Macromolecules from Atomic Coordinates," *J. Appl. Crystallogr.*, vol. 28, pp. 768–773, 1995.

## **Appendix**

### **REPRINT PERMISSION LETTERS**

The following pages contain permission letters for the three reprinted figures in the thesis. These figures are: Figure 12 by Krueger *et al.* [16], Figure 24 (left panel) by Angelo *et al.* [19], and Figure 24 (right panel) by Angelo *et al.* [20].

**ELSEVIER LICENSE  
TERMS AND CONDITIONS**

Apr 14, 2014

---

This is a License Agreement between Stijn HS Koshari ("You") and Elsevier ("Elsevier") provided by Copyright Clearance Center ("CCC"). The license consists of your order details, the terms and conditions provided by Elsevier, and the payment terms and conditions.

**All payments must be made in full to CCC. For payment instructions, please see information listed at the bottom of this form.**

Supplier	Elsevier Limited The Boulevard, Langford Lane Kidlington, Oxford, OX5 1GB, UK
Registered Company Number	1982084
Customer name	Stijn HS Koshari
Customer address	316 Chickory Way Newark, DE 19711
License number	3367840430045
License date	Apr 14, 2014
Licensed content publisher	Elsevier
Licensed content publication	Biophysical Chemistry
Licensed content title	Small angle neutron scattering studies of structural characteristics of agarose gels
Licensed content author	Susan Krueger, Anna Ploplis Andrews, Ralph Nossal
Licensed content date	December 1994
Licensed content volume number	53
Licensed content issue number	1-2
Number of pages	10
Start Page	85
End Page	94
Type of Use	reuse in a thesis/dissertation
Intended publisher of new work	other
Portion	figures/tables/illustrations
Number of figures/tables /illustrations	1
Format	both print and electronic
Are you the author of this Elsevier article?	No
Will you be translating?	No

Title of your thesis/dissertation	Characterization of Lysozyme Adsorption in Cellulosic Chromatographic Materials using Small-Angle Neutron Scattering
Expected completion date	Apr 2014
Estimated size (number of pages)	77
Elsevier VAT number	GB 494 6272 12
Permissions price	0.00 USD
VAT/Local Sales Tax	0.00 USD / 0.00 GBP
Total	0.00 USD
<a href="#">Terms and Conditions</a>	

## INTRODUCTION

1. The publisher for this copyrighted material is Elsevier. By clicking "accept" in connection with completing this licensing transaction, you agree that the following terms and conditions apply to this transaction (along with the Billing and Payment terms and conditions established by Copyright Clearance Center, Inc. ("CCC"), at the time that you opened your Rightslink account and that are available at any time at <http://myaccount.copyright.com>).

## GENERAL TERMS

2. Elsevier hereby grants you permission to reproduce the aforementioned material subject to the terms and conditions indicated.

3. Acknowledgement: If any part of the material to be used (for example, figures) has appeared in our publication with credit or acknowledgement to another source, permission must also be sought from that source. If such permission is not obtained then that material may not be included in your publication/copies. Suitable acknowledgement to the source must be made, either as a footnote or in a reference list at the end of your publication, as follows:

“Reprinted from Publication title, Vol /edition number, Author(s), Title of article / title of chapter, Pages No., Copyright (Year), with permission from Elsevier [OR APPLICABLE SOCIETY COPYRIGHT OWNER].” Also Lancet special credit -“Reprinted from The Lancet, Vol. number, Author(s), Title of article, Pages No., Copyright (Year), with permission from Elsevier.”

4. Reproduction of this material is confined to the purpose and/or media for which permission is hereby given.

5. Altering/Modifying Material: Not Permitted. However figures and illustrations may be altered/adapted minimally to serve your work. Any other abbreviations, additions, deletions and/or any other alterations shall be made only with prior written authorization of Elsevier Ltd. (Please contact Elsevier at [permissions@elsevier.com](mailto:permissions@elsevier.com))

6. If the permission fee for the requested use of our material is waived in this instance, please be advised that your future requests for Elsevier materials may attract a fee.

7. **Reservation of Rights:** Publisher reserves all rights not specifically granted in the combination of (i) the license details provided by you and accepted in the course of this licensing transaction, (ii) these terms and conditions and (iii) CCC's Billing and Payment terms and conditions.

8. **License Contingent Upon Payment:** While you may exercise the rights licensed immediately upon issuance of the license at the end of the licensing process for the transaction, provided that you have disclosed complete and accurate details of your proposed use, no license is finally effective unless and until full payment is received from you (either by publisher or by CCC) as provided in CCC's Billing and Payment terms and conditions. If full payment is not received on a timely basis, then any license preliminarily granted shall be deemed automatically revoked and shall be void as if never granted. Further, in the event that you breach any of these terms and conditions or any of CCC's Billing and Payment terms and conditions, the license is automatically revoked and shall be void as if never granted. Use of materials as described in a revoked license, as well as any use of the materials beyond the scope of an unrevoked license, may constitute copyright infringement and publisher reserves the right to take any and all action to protect its copyright in the materials.

9. **Warranties:** Publisher makes no representations or warranties with respect to the licensed material.

10. **Indemnity:** You hereby indemnify and agree to hold harmless publisher and CCC, and their respective officers, directors, employees and agents, from and against any and all claims arising out of your use of the licensed material other than as specifically authorized pursuant to this license.

11. **No Transfer of License:** This license is personal to you and may not be sublicensed, assigned, or transferred by you to any other person without publisher's written permission.

12. **No Amendment Except in Writing:** This license may not be amended except in a writing signed by both parties (or, in the case of publisher, by CCC on publisher's behalf).

13. **Objection to Contrary Terms:** Publisher hereby objects to any terms contained in any purchase order, acknowledgment, check endorsement or other writing prepared by you, which terms are inconsistent with these terms and conditions or CCC's Billing and Payment terms and conditions. These terms and conditions, together with CCC's Billing and Payment terms and conditions (which are incorporated herein), comprise the entire agreement between you and publisher (and CCC) concerning this licensing transaction. In the event of any conflict between your obligations established by these terms and conditions and those established by CCC's Billing and Payment terms and conditions, these terms and conditions shall control.

14. **Revocation:** Elsevier or Copyright Clearance Center may deny the permissions described in this License at their sole discretion, for any reason or no reason, with a full refund payable to you. Notice of such denial will be made using the contact information provided by you. Failure to receive such notice will not alter or invalidate the denial. In no event will Elsevier or Copyright Clearance Center be responsible or liable for any costs, expenses or damage incurred by you as a result of a denial of your permission request, other than a refund of the

amount(s) paid by you to Elsevier and/or Copyright Clearance Center for denied permissions.

## LIMITED LICENSE

The following terms and conditions apply only to specific license types:

**15. Translation:** This permission is granted for non-exclusive world **English** rights only unless your license was granted for translation rights. If you licensed translation rights you may only translate this content into the languages you requested. A professional translator must perform all translations and reproduce the content word for word preserving the integrity of the article. If this license is for use of 1 or 2 figures then permission is granted for non-exclusive world rights in all languages.

**16. Posting licensed content on any Website:** The following terms and conditions apply as follows: Licensing material from an Elsevier journal: All content posted to the web site must maintain the copyright information line on the bottom of each image; A hyper-text must be included to the Homepage of the journal from which you are licensing at <http://www.sciencedirect.com/science/journal/xxxxx> or the Elsevier homepage for books at <http://www.elsevier.com>; Central Storage: This license does not include permission for a scanned version of the material to be stored in a central repository such as that provided by Heron/XanEdu.

Licensing material from an Elsevier book: A hyper-text link must be included to the Elsevier homepage at <http://www.elsevier.com>. All content posted to the web site must maintain the copyright information line on the bottom of each image.

**Posting licensed content on Electronic reserve:** In addition to the above the following clauses are applicable: The web site must be password-protected and made available only to bona fide students registered on a relevant course. This permission is granted for 1 year only. You may obtain a new license for future website posting.

**For journal authors:** the following clauses are applicable in addition to the above: Permission granted is limited to the author accepted manuscript version\* of your paper.

**\*Accepted Author Manuscript (AAM) Definition:** An accepted author manuscript (AAM) is the author's version of the manuscript of an article that has been accepted for publication and which may include any author-incorporated changes suggested through the processes of submission processing, peer review, and editor-author communications. AAMs do not include other publisher value-added contributions such as copy-editing, formatting, technical enhancements and (if relevant) pagination.

You are not allowed to download and post the published journal article (whether PDF or HTML, proof or final version), nor may you scan the printed edition to create an electronic version. A hyper-text must be included to the Homepage of the journal from which you are licensing at <http://www.sciencedirect.com/science/journal/xxxxx>. As part of our normal production process, you will receive an e-mail notice when your article appears on Elsevier's online service ScienceDirect ([www.sciencedirect.com](http://www.sciencedirect.com)). That e-mail will include the article's Digital Object Identifier (DOI). This number provides the electronic link to the published article and should be included in the posting of your personal version. We ask that

you wait until you receive this e-mail and have the DOI to do any posting.

**Posting to a repository:** Authors may post their AAM immediately to their employer's institutional repository for internal use only and may make their manuscript publically available after the journal-specific embargo period has ended.

Please also refer to Elsevier's Article Posting Policy for further information.

**18. For book authors** the following clauses are applicable in addition to the above: Authors are permitted to place a brief summary of their work online only.. You are not allowed to download and post the published electronic version of your chapter, nor may you scan the printed edition to create an electronic version. Posting to a repository: Authors are permitted to post a summary of their chapter only in their institution's repository.

**20. Thesis/Dissertation:** If your license is for use in a thesis/dissertation your thesis may be submitted to your institution in either print or electronic form. Should your thesis be published commercially, please apply for permission. These requirements include permission for the Library and Archives of Canada to supply single copies, on demand, of the complete thesis and include permission for UMI to supply single copies, on demand, of the complete thesis. Should your thesis be published commercially, please apply for permission.

### **Elsevier Open Access Terms and Conditions**

Elsevier publishes Open Access articles in both its Open Access journals and via its Open Access articles option in subscription journals.

Authors publishing in an Open Access journal or who choose to make their article Open Access in an Elsevier subscription journal select one of the following Creative Commons user licenses, which define how a reader may reuse their work: Creative Commons Attribution License (CC BY), Creative Commons Attribution – Non Commercial - Share Alike (CC BY NC SA) and Creative Commons Attribution – Non Commercial – No Derivatives (CC BY NC ND)

### **Terms & Conditions applicable to all Elsevier Open Access articles:**

Any reuse of the article must not represent the author as endorsing the adaptation of the article nor should the article be modified in such a way as to damage the author's honour or reputation.

The author(s) must be appropriately credited.

If any part of the material to be used (for example, figures) has appeared in our publication with credit or acknowledgement to another source it is the responsibility of the user to ensure their reuse complies with the terms and conditions determined by the rights holder.

### **Additional Terms & Conditions applicable to each Creative Commons user license:**

**CC BY:** You may distribute and copy the article, create extracts, abstracts, and other revised versions, adaptations or derivative works of or from an article (such as a translation), to include in a collective work (such as an anthology), to text or data mine the article, including for commercial purposes without permission from Elsevier

**CC BY NC SA:** For non-commercial purposes you may distribute and copy the article, create extracts, abstracts and other revised versions, adaptations or derivative works of or from an article (such as a translation), to include in a collective work (such as an anthology), to text and data mine the article and license new adaptations or creations under identical terms without permission from Elsevier

**CC BY NC ND:** For non-commercial purposes you may distribute and copy the article and include it in a collective work (such as an anthology), provided you do not alter or modify the article, without permission from Elsevier

Any commercial reuse of Open Access articles published with a CC BY NC SA or CC BY NC ND license requires permission from Elsevier and will be subject to a fee.

Commercial reuse includes:

- Promotional purposes (advertising or marketing)
- Commercial exploitation ( e.g. a product for sale or loan)
- Systematic distribution (for a fee or free of charge)

Please refer to Elsevier's Open Access Policy for further information.

## 21. Other Conditions:

v1.7

**If you would like to pay for this license now, please remit this license along with your payment made payable to "COPYRIGHT CLEARANCE CENTER" otherwise you will be invoiced within 48 hours of the license date. Payment should be in the form of a check or money order referencing your account number and this invoice number RLNK501278011.**

**Once you receive your invoice for this order, you may pay your invoice by credit card. Please follow instructions provided at that time.**

**Make Payment To:  
Copyright Clearance Center  
Dept 001  
P.O. Box 843006  
Boston, MA 02284-3006**

**For suggestions or comments regarding this order, contact RightsLink Customer**



**Support:** [customercare@copyright.com](mailto:customercare@copyright.com) or +1-877-622-5543 (toll free in the US) or +1-978-646-2777.

**Gratis licenses (referencing \$0 in the Total field) are free. Please retain this printable license for your reference. No payment is required.**

---

---

## ELSEVIER LICENSE TERMS AND CONDITIONS

Apr 14, 2014

---

This is a License Agreement between Stijn HS Koshari ("You") and Elsevier ("Elsevier") provided by Copyright Clearance Center ("CCC"). The license consists of your order details, the terms and conditions provided by Elsevier, and the payment terms and conditions.

**All payments must be made in full to CCC. For payment instructions, please see information listed at the bottom of this form.**

Supplier	Elsevier Limited The Boulevard, Langford Lane Kidlington, Oxford, OX5 1GB, UK
Registered Company Number	1982084
Customer name	Stijn HS Koshari
Customer address	316 Chickory Way Newark, DE 19711
License number	3367840592848
License date	Apr 14, 2014
Licensed content publisher	Elsevier
Licensed content publication	Journal of Chromatography A
Licensed content title	Characterization of cross-linked cellulosic ion-exchange adsorbents: 1. Structural properties
Licensed content author	James M. Angelo, Aleksandar Cvetkovic, Rene Gantier, Abraham M. Lenhoff
Licensed content date	6 December 2013
Licensed content volume number	1319
Licensed content issue number	
Number of pages	11
Start Page	46
End Page	56
Type of Use	reuse in a thesis/dissertation
Intended publisher of new work	other
Portion	figures/tables/illustrations
Number of figures/tables /illustrations	1
Format	both print and electronic
Are you the author of this Elsevier article?	No

Will you be translating?	No
Title of your thesis/dissertation	Characterization of Lysozyme Adsorption in Cellulosic Chromatographic Materials using Small-Angle Neutron Scattering
Expected completion date	Apr 2014
Estimated size (number of pages)	77
Elsevier VAT number	GB 494 6272 12
Permissions price	0.00 USD
VAT/Local Sales Tax	0.00 USD / 0.00 GBP
Total	0.00 USD
Terms and Conditions	

## INTRODUCTION

1. The publisher for this copyrighted material is Elsevier. By clicking "accept" in connection with completing this licensing transaction, you agree that the following terms and conditions apply to this transaction (along with the Billing and Payment terms and conditions established by Copyright Clearance Center, Inc. ("CCC"), at the time that you opened your Rightslink account and that are available at any time at <http://myaccount.copyright.com>).

## GENERAL TERMS

2. Elsevier hereby grants you permission to reproduce the aforementioned material subject to the terms and conditions indicated.

3. Acknowledgement: If any part of the material to be used (for example, figures) has appeared in our publication with credit or acknowledgement to another source, permission must also be sought from that source. If such permission is not obtained then that material may not be included in your publication/copies. Suitable acknowledgement to the source must be made, either as a footnote or in a reference list at the end of your publication, as follows:

"Reprinted from Publication title, Vol /edition number, Author(s), Title of article / title of chapter, Pages No., Copyright (Year), with permission from Elsevier [OR APPLICABLE SOCIETY COPYRIGHT OWNER]." Also Lancet special credit - "Reprinted from The Lancet, Vol. number, Author(s), Title of article, Pages No., Copyright (Year), with permission from Elsevier."

4. Reproduction of this material is confined to the purpose and/or media for which permission is hereby given.

5. Altering/Modifying Material: Not Permitted. However figures and illustrations may be altered/adapted minimally to serve your work. Any other abbreviations, additions, deletions and/or any other alterations shall be made only with prior written authorization of Elsevier Ltd. (Please contact Elsevier at [permissions@elsevier.com](mailto:permissions@elsevier.com))

6. If the permission fee for the requested use of our material is waived in this instance, please

be advised that your future requests for Elsevier materials may attract a fee.

7. Reservation of Rights: Publisher reserves all rights not specifically granted in the combination of (i) the license details provided by you and accepted in the course of this licensing transaction, (ii) these terms and conditions and (iii) CCC's Billing and Payment terms and conditions.

8. License Contingent Upon Payment: While you may exercise the rights licensed immediately upon issuance of the license at the end of the licensing process for the transaction, provided that you have disclosed complete and accurate details of your proposed use, no license is finally effective unless and until full payment is received from you (either by publisher or by CCC) as provided in CCC's Billing and Payment terms and conditions. If full payment is not received on a timely basis, then any license preliminarily granted shall be deemed automatically revoked and shall be void as if never granted. Further, in the event that you breach any of these terms and conditions or any of CCC's Billing and Payment terms and conditions, the license is automatically revoked and shall be void as if never granted. Use of materials as described in a revoked license, as well as any use of the materials beyond the scope of an unrevoked license, may constitute copyright infringement and publisher reserves the right to take any and all action to protect its copyright in the materials.

9. Warranties: Publisher makes no representations or warranties with respect to the licensed material.

10. Indemnity: You hereby indemnify and agree to hold harmless publisher and CCC, and their respective officers, directors, employees and agents, from and against any and all claims arising out of your use of the licensed material other than as specifically authorized pursuant to this license.

11. No Transfer of License: This license is personal to you and may not be sublicensed, assigned, or transferred by you to any other person without publisher's written permission.

12. No Amendment Except in Writing: This license may not be amended except in a writing signed by both parties (or, in the case of publisher, by CCC on publisher's behalf).

13. Objection to Contrary Terms: Publisher hereby objects to any terms contained in any purchase order, acknowledgment, check endorsement or other writing prepared by you, which terms are inconsistent with these terms and conditions or CCC's Billing and Payment terms and conditions. These terms and conditions, together with CCC's Billing and Payment terms and conditions (which are incorporated herein), comprise the entire agreement between you and publisher (and CCC) concerning this licensing transaction. In the event of any conflict between your obligations established by these terms and conditions and those established by CCC's Billing and Payment terms and conditions, these terms and conditions shall control.

14. Revocation: Elsevier or Copyright Clearance Center may deny the permissions described in this License at their sole discretion, for any reason or no reason, with a full refund payable to you. Notice of such denial will be made using the contact information provided by you. Failure to receive such notice will not alter or invalidate the denial. In no event will Elsevier or Copyright Clearance Center be responsible or liable for any costs, expenses or damage

incurred by you as a result of a denial of your permission request, other than a refund of the amount(s) paid by you to Elsevier and/or Copyright Clearance Center for denied permissions.

### LIMITED LICENSE

The following terms and conditions apply only to specific license types:

**15. Translation:** This permission is granted for non-exclusive world **English** rights only unless your license was granted for translation rights. If you licensed translation rights you may only translate this content into the languages you requested. A professional translator must perform all translations and reproduce the content word for word preserving the integrity of the article. If this license is for use of 1 or 2 figures then permission is granted for non-exclusive world rights in all languages.

**16. Posting licensed content on any Website:** The following terms and conditions apply as follows: Licensing material from an Elsevier journal: All content posted to the web site must maintain the copyright information line on the bottom of each image; A hyper-text must be included to the Homepage of the journal from which you are licensing at <http://www.sciencedirect.com/science/journal/xxxxx> or the Elsevier homepage for books at <http://www.elsevier.com>; Central Storage: This license does not include permission for a scanned version of the material to be stored in a central repository such as that provided by Heron/XanEdu.

Licensing material from an Elsevier book: A hyper-text link must be included to the Elsevier homepage at <http://www.elsevier.com>. All content posted to the web site must maintain the copyright information line on the bottom of each image.

**Posting licensed content on Electronic reserve:** In addition to the above the following clauses are applicable: The web site must be password-protected and made available only to bona fide students registered on a relevant course. This permission is granted for 1 year only. You may obtain a new license for future website posting.

**For journal authors:** the following clauses are applicable in addition to the above: Permission granted is limited to the author accepted manuscript version\* of your paper.

**\*Accepted Author Manuscript (AAM) Definition:** An accepted author manuscript (AAM) is the author's version of the manuscript of an article that has been accepted for publication and which may include any author-incorporated changes suggested through the processes of submission processing, peer review, and editor-author communications. AAMs do not include other publisher value-added contributions such as copy-editing, formatting, technical enhancements and (if relevant) pagination.

You are not allowed to download and post the published journal article (whether PDF or HTML, proof or final version), nor may you scan the printed edition to create an electronic version. A hyper-text must be included to the Homepage of the journal from which you are licensing at <http://www.sciencedirect.com/science/journal/xxxxx>. As part of our normal production process, you will receive an e-mail notice when your article appears on Elsevier's online service ScienceDirect ([www.sciencedirect.com](http://www.sciencedirect.com)). That e-mail will include the article's Digital Object Identifier (DOI). This number provides the electronic link to the

published article and should be included in the posting of your personal version. We ask that you wait until you receive this e-mail and have the DOI to do any posting.

**Posting to a repository:** Authors may post their AAM immediately to their employer's institutional repository for internal use only and may make their manuscript publicly available after the journal-specific embargo period has ended.

Please also refer to Elsevier's Article Posting Policy for further information.

**18. For book authors** the following clauses are applicable in addition to the above: Authors are permitted to place a brief summary of their work online only.. You are not allowed to download and post the published electronic version of your chapter, nor may you scan the printed edition to create an electronic version. Posting to a repository: Authors are permitted to post a summary of their chapter only in their institution's repository.

**20. Thesis/Dissertation:** If your license is for use in a thesis/dissertation your thesis may be submitted to your institution in either print or electronic form. Should your thesis be published commercially, please apply for permission. These requirements include permission for the Library and Archives of Canada to supply single copies, on demand, of the complete thesis and include permission for UMI to supply single copies, on demand, of the complete thesis. Should your thesis be published commercially, please apply for permission.

### **Elsevier Open Access Terms and Conditions**

Elsevier publishes Open Access articles in both its Open Access journals and via its Open Access articles option in subscription journals.

Authors publishing in an Open Access journal or who choose to make their article Open Access in an Elsevier subscription journal select one of the following Creative Commons user licenses, which define how a reader may reuse their work: Creative Commons Attribution License (CC BY), Creative Commons Attribution – Non Commercial – Share Alike (CC BY NC SA) and Creative Commons Attribution – Non Commercial – No Derivatives (CC BY NC ND)

### **Terms & Conditions applicable to all Elsevier Open Access articles:**

Any reuse of the article must not represent the author as endorsing the adaptation of the article nor should the article be modified in such a way as to damage the author's honour or reputation.

The author(s) must be appropriately credited.

If any part of the material to be used (for example, figures) has appeared in our publication with credit or acknowledgement to another source it is the responsibility of the user to ensure their reuse complies with the terms and conditions determined by the rights holder.

### **Additional Terms & Conditions applicable to each Creative Commons user license:**

**CC BY:** You may distribute and copy the article, create extracts, abstracts, and other revised versions, adaptations or derivative works of or from an article (such as a translation), to include in a collective work (such as an anthology), to text or data mine the article, including for commercial purposes without permission from Elsevier

**CC BY NC SA:** For non-commercial purposes you may distribute and copy the article, create extracts, abstracts and other revised versions, adaptations or derivative works of or from an article (such as a translation), to include in a collective work (such as an anthology), to text and data mine the article and license new adaptations or creations under identical terms without permission from Elsevier

**CC BY NC ND:** For non-commercial purposes you may distribute and copy the article and include it in a collective work (such as an anthology), provided you do not alter or modify the article, without permission from Elsevier

Any commercial reuse of Open Access articles published with a CC BY NC SA or CC BY NC ND license requires permission from Elsevier and will be subject to a fee.

Commercial reuse includes:

- Promotional purposes (advertising or marketing)
- Commercial exploitation ( e.g. a product for sale or loan)
- Systematic distribution (for a fee or free of charge)

Please refer to Elsevier's Open Access Policy for further information.

## 21. Other Conditions:

v1.7

**If you would like to pay for this license now, please remit this license along with your payment made payable to "COPYRIGHT CLEARANCE CENTER" otherwise you will be invoiced within 48 hours of the license date. Payment should be in the form of a check or money order referencing your account number and this invoice number RLNK501278014.**

**Once you receive your invoice for this order, you may pay your invoice by credit card. Please follow instructions provided at that time.**

**Make Payment To:  
Copyright Clearance Center  
Dept 001  
P.O. Box 843006  
Boston, MA 02284-3006**

**For suggestions or comments regarding this order, contact RightsLink Customer**

**Support:** [customercare@copyright.com](mailto:customercare@copyright.com) or +1-877-622-5543 (toll free in the US) or +1-978-646-2777.

**Gratis licenses (referencing \$0 in the Total field) are free. Please retain this printable license for your reference. No payment is required.**

---

---



James M. Angelo  
Colburn Laboratory  
150 Academy Street  
Newark, DE 19716  
USA

16 April 2014

### **Reprint Permission Letter**

I hereby grant Stijn H.S. Koshari permission to reproduce the material specified below for his Master's Thesis.

*Content title:*

Characterization of cross-linked cellulosic ion-exchange adsorbents: 2. Protein Sorption and Transport

*Content author:*

James M. Angelo, Aleksandar Cvetkovic, Rene Gantier, Abraham M. Lenhoff

*Portion:*

One (1) figure: SEM image of Q HyperCel

*Type of use:*

Reuse in a thesis

*Format:*

Both print and electronic

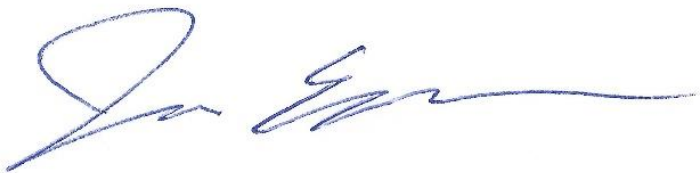
*Title of the thesis:*

Characterization of Lysozyme Adsorption in Cellulosic Chromatographic Materials using Small-Angle Neutron Scattering

*Expected completion date:*

April 2014

Signed,



James M. Angelo